STUDY OF THE DOUBLE-CONE RING GASKET

by

Chao-lin Lou

B.Sc., National Taiwan University, 1963

A Thesis Submitted in Partial Fulfillment of the

Requirements for the Degree of

Master of Applied Science

In the Department

of

Mechanical Engineering

We accept this thesis as conforming to

the required standard

THE UNIVERSITY OF BRITISH COLUMBIA

August, 1967

In presenting this thesis in partial fulfilment of the requirements

for an advanced degree at the University of British Columbia, I agree

that the Library shall make it freely available for reference and

Study. I further agree that permission for extensive copying of this

thesis for scholarly purposes may be granted by the Head of my

Department or by his representatives. It is understood that copying

or publication of this thesis for financial gain shall not be allowed

without my written permission.

Department of <u>Mechanical Engineering</u>

The University of British Columbia
Vancouver 8, Canada

Date <u>August 25, 1967</u>

ABSTRACT

The double-cone ring gasket used as a static seal for high pressure operates on the principle of unsupported area by which the pressure applied to the gasket produces a large pressure at the seating surfaces thus maintaining a tight joint.

An analysis based on elastic behaviour and simplifying assumptions is developed for predicting the sealing forces and the strains in the gasket.

An apparatus was built for testing the effectiveness of the gasket for sealing pressures to 10,000 psi. Gaskets of several different proportions were tested and all were found to seal satisfactorily. Strain measurements made during the tests showed satisfactory agreement with predicted values for the assembly condition, but there were discrepancies between the predicted and observed values for the gaskets under pressure. These discrepancies indicate that the simple assumptions used in the analysis are not sufficiently accurate.

The general conclusions are that the double-cone ring gasket is satisfactory for high pressure static seals and that the proportions of the ring cross section are not critical to the effectiveness of the seal.

ACKNOWLEDGEMENT

CONTENTS

LIST OF ILLUSTRATIONS

LIST OF TABLES

LIST OF SYMBOLS

b: Half-width of ring gasket, in.

c_e: Radial crush of ring gasket at edges.

c_o: Total radial crush at edges of a ring gasket in the assembled state.

C_1, C_2, C_3, C_4:   Constants of integration.

D: Flexural rigidity, $Eh^3/12(1-\mu^2)$.

e: Width of seating bevel, in.

E: Young's modulus, lb/in^2.

g: Initial stand-off of flanges, in.

G: Shear modulus, $G = E/2(1+\mu)$.

h: Thickness of ring wall, in.

k: Pressure-contact ratio, $k = e/h$.

K_c, K_p: Coefficients related to $(\frac{N}{Eh})$

M: Bending moment in ring wall, lb-in/in.

M*:   Moment term, $M* = Nhb^2\sin\theta/2Dr$.

N: Sealing force normal per unit length of ring circumference, lb/in.

p: Internal pressure applied in ring gasket, positive outward, lb/in^2.

$\bar{P}$:   Pressure-force term, $P = p(1-h/2r) - \mu(N\sin\theta+ph)/r$.

P*:   Particular integral.

r: Mean radius of ring, in.

R: Maximum radius of flange bore, in.

s_h: Hoop compression in ring wall, lb/in^2.

V: Shear force in ring wall, lb/in.

w: Total radial deflection of ring gasket, positive inward, in.

w_b: Radial deflection of ring gasket due to bending, in.

w_s: Radial deflection of ring gasket due to shear, in.

x: Co-ordinate in axial direction of ring gasket, in.

ε_0: Tangential strain at the centroid of the axial cross-section of ring gasket.

ε_s: Tangential strain on outer surface of ring ($x=0$).

μ: Poisson's ratio.

ρ, α: Design parameters of ring, $\rho = r/h$ and $\alpha = b/h$.

θ: Inclination angle of ring bevels.

η_c, η_p: Coefficients related to tangential strain of ring gasket.

$\omega, \xi, \lambda, \gamma, \Gamma_0, \Gamma_1, \Gamma_2$: Operation parameters and notations defined for simplicity.

CHAPTER I

INTRODUCTION

1.1 Purpose of Investigation

It is obvious that the most vital problem which must be faced in every high-pressure application is the prevention of leaks. This means in every case some form of sealing.

To prevent the migration of high-pressure fluid across the joint of a vessel or an assembly where no relative motion occurs between the joined parts, a great many forms of static seals have been developed in the past years. One of these, the double-cone ring gasket, is the subject of the present study. This gasket is a pressure-energized ring seal used in various fields of high pressures. Although a large amount of information about such ring seals have been published, much research work is yet to be done. Accordingly, to study the behaviour of the double-cone ring gasket as a static seal with a view to determining the optimum design properties and conditions becomes the original object of this research project.

1.2 Outline of Thesis

In the present thesis, a historical review of the design concepts of high-pressure gaskets is reported, and the basic design principle of the double-cone ring gasket is discussed.

A simplified elastic analysis is developed, and equations for predicting the sealing forces and the tangential strains in the double-cone ring gaskets are derived as the results of this analysis.

For the experimental part of the investigation, double-cone ring gasket models are made and tested. The physical properties of

model materials, the design details of the models, the testing apparatus and the test procedure are separately described in the thesis. Then the results of the strain-measurements made in testing the ring gasket models are presented in graphic form and compared with the theoretically predicted values. In addition, the observations on the performance characteristics of the tested models are also reported. These observations lead to some design criteria for the double-cone ring gasket.

Finally, a few statements serving as the general conclusions of the present investigation are mentioned, and suggestions which may be helpful to further researches on the behaviour of double-cone ring gasket are stated.

CHAPTER II

THE DESIGN PRINCIPLE OF DOUBLE-CONE RING GASKET

2.1 Historical Review of High-Pressure Gasket Design

Three distinct stages in the evolution of high-pressure gasket design may be distinguished [1]*. The design concept developed in each of these three stages can be discussed separately by way of introducing the problem of sealing the pipe connection in a high-pressure system.

A schematic illustration of the most primitive design is shown in Figure 1. In this design, the sealing pressure exerted on the sealing surfaces between the gasket and the rigid members completely depends on the initial bolt load applied in assembling this pipe connection. This design has two shortcomings.
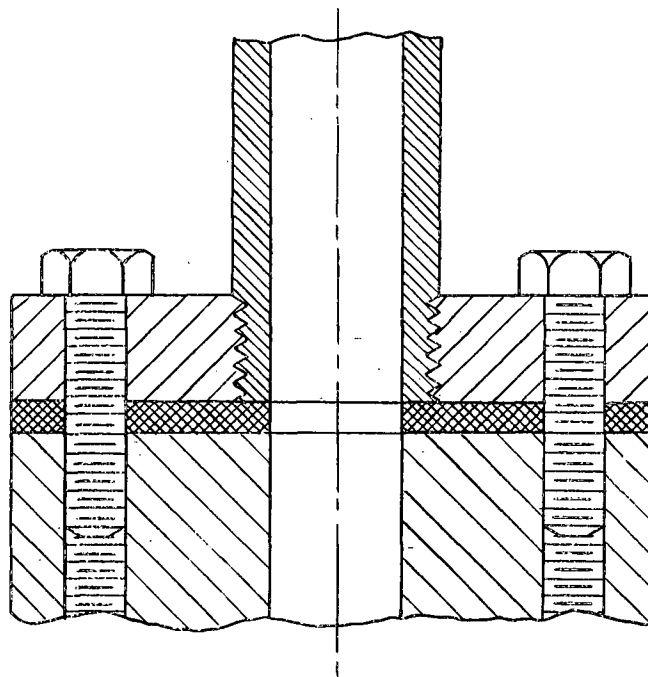
FIGURE 1 Most Primitive Design of High-Pressure Gasket

---

*Numbers in brackets identify references at the end of thesis.

The first one is that during the assembly process, in order to make the gasket proof against high pressure, the gasket must be very tightly compressed; as a consequence, the gasket might flow sidewise, either into the interior of the pipe or to the outside. Another shortcoming of this design is that, when the hydrostatic pressure in the pipe is very high, the gasket will be blown out by it.

The second stage of evolution is shown in Figure 2. In this
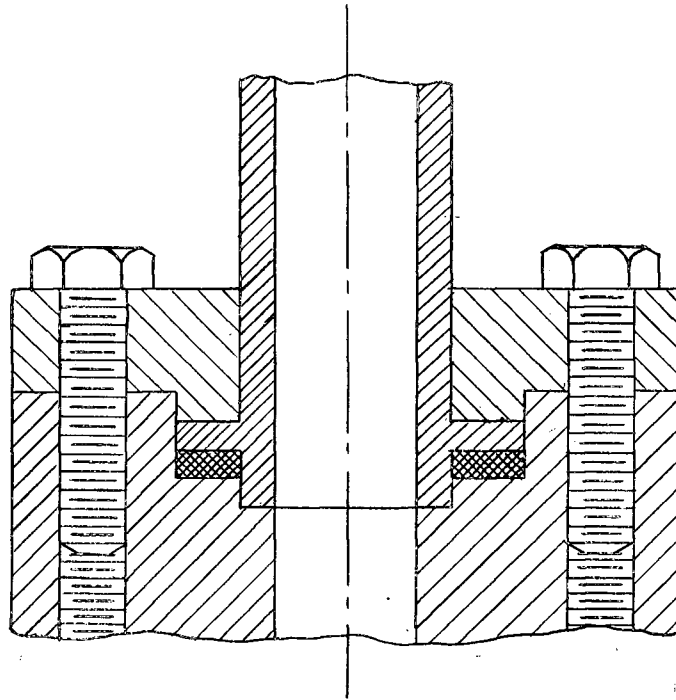
FIGURE 2 Amagat's Type of Fully Enclosed Gasket

improved design, a flange is formed on the end of the pipe, and this pipe flange enters a recess in such a way that the gasket is entirely enclosed by rigid metal walls. Therefore, the gasket can neither flow sidewise under initial bolt load, nor can it be blown out by the hydrostatic pressure contained. The gaskets of such a design are commonly known as the Amagat's type of fully-enclosed gaskets. However, the upper pressure limit at which an Amagat's gasket can be effectively used is still

set by the intensity of the initial bolt load imposed in assembly. When
the hydrostatic pressure in the pipe has reached an intensity equal to
that initially exerted on the sealing surfaces by the screws, there is
balance. Any further increase of hydrostatic pressure above this limit
will cause the gasket to shrink away from the containing wall and produce
a leak.

Figure 3 shows the gasket design in the third stage of evolution.
At first sight, it seems that this design appears to be only a modification
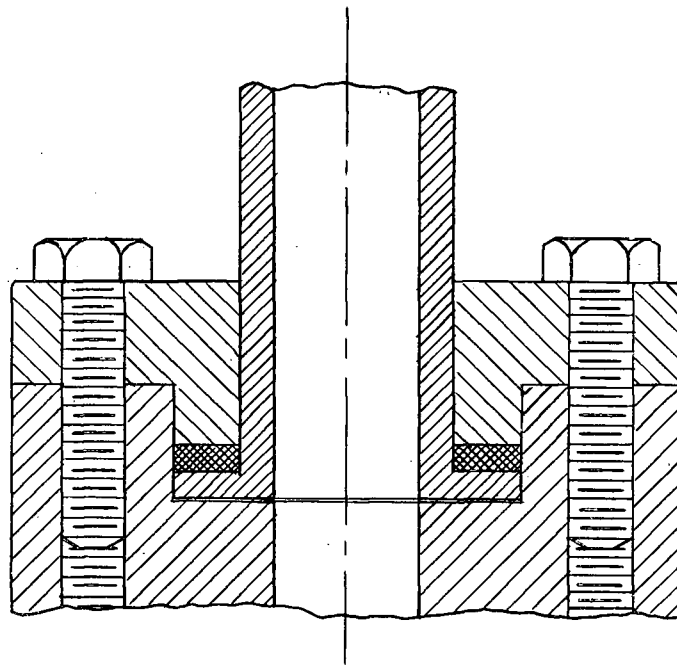
FIGURE 3 - High-Pressure Gasket Design Utilizing
the Principle of Unsupported Area

of the one shown in Figure 2. The location of gasket has been changed
from the front to the back side of the pipe flange. However, this
apparently trivial change has introduced a very important change in
the design concept of high-pressure gasket, and has made the conventional,
compressive gasket into one utilizing the principle of unsupported area.
This principle forms the basic design concept of the double-cone ring

gasket and many other pressure-energized gaskets. The next section will be devoted to describing this principle in detail.

2.2 The Principle of Unsupported Area

The principle of unsupported area can be stated as [1][2][3][5]: "If the geometrical design of a gasket assembly is such that there exists a certain amount of unsupported area, then the intensity of the sealing pressure on the sealing surface of the gasket can automatically be maintained at a fixed percentage higher than the pressure intensity in the contained fluid, and leak of the fluid cannot occur as long as the retaining walls of this gasket assembly hold."

In the design shown in Figure 3, the unsupported area is the area of the cross-section of the pipe. This principle of unsupported area is commonly credited to P.W. Bridgman, and has been widely employed in many high-pressure gasket designs. A survey of the existing high-pressure gaskets reveals that most of the pressure-energized gaskets used in various fields of very high pressures utilize this principle [8][9].

2.3 Design Features of the Double-Cone Ring Gasket

The double-cone ring type of gasket was originally developed in Germany for high-pressure reactors. As implied by its name, this gasket is essentially a metallic ring joint made from forged aluminium or mild steel, consisting of two cone type seating bevels which form part of the outer surface. The schematic illustration of such a ring joint is shown in Figure 4.
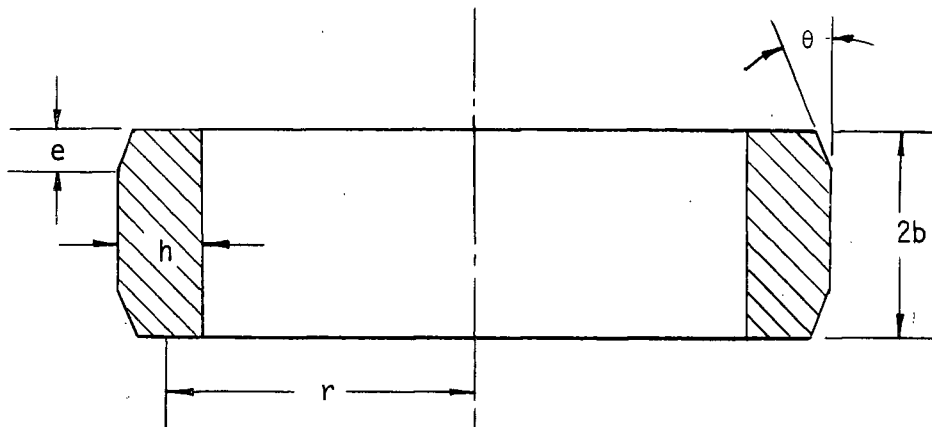
r: Mean radius of ring

b: Half-width of ring

h: Thickness of ring

e: Width of seating bevel

θ: Inclination angle of seating bevel

k: Pressure-contact ratio

$\rho = r/h$ ⎫
$\alpha = b/h$ ⎭ Design parameters of ring

FIGURE 4   A Double-Cone Ring Gasket

When used as a static seal, this ring gasket is placed between two flanges of specific design, as shown in Figure 5. In order to create the necessary initial seal, so that the hydrostatic pressure subsequently applied to this assembly can act on the inner surface of ring only, the flanges and the ring are so dimensioned that the seating bevels of ring come in contact with the sealing surfaces of flanges when the flanges have a standoff g (see Figure 5). Tightening the studs swages the ring inward until the flanges are face to face. Under this bolt-up condition, no hydrostatic pressure exists and the full bolt load is carried by the slightly coned ring. Figure 6 shows a double-cone ring gasket in the assembled state.
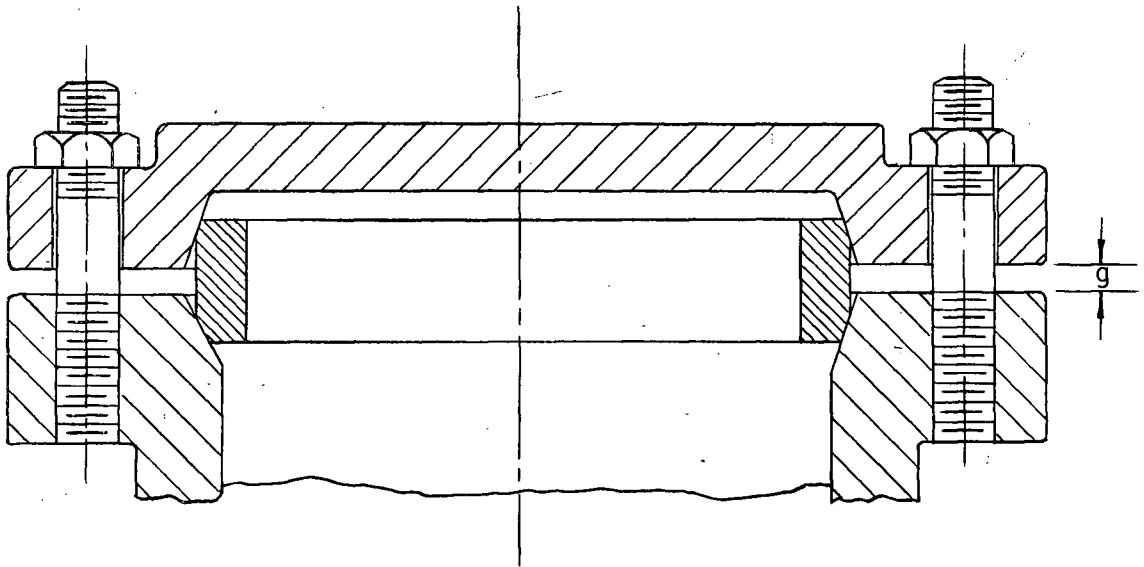
FIGURE 5 The Double-Cone Ring Gasket and Flanges Before Assembly
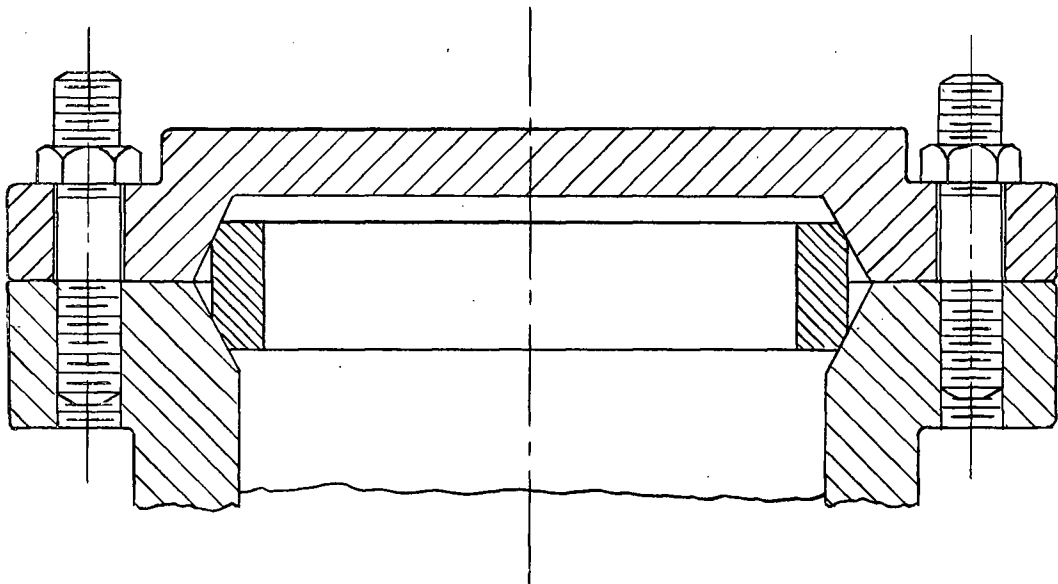
FIGURE 6 The Double-Cone Ring Gasket in the Assembled State

After the flanges are tightly bolted and the ring has been properly seated, hydrostatic pressure can then be applied. A portion of the applied pressure, which is acting on the inner surface of ring, expands the ring into the sealing surfaces of flanges and forces it to maintain a seal. Since there exists an unsupported area in this gasket design, which is equal to the difference between the inner surface of ring and the   projected area of ring bevels, the increase in the intensity of sealing pressure will be higher than the increase in the intensity of applied pressure. Therefore, an effective seal can be retained no matter how high the applied pressure.

Since the ring expansion mentioned in the last paragraph, along with the hydrostatic pressure acting on the flat portions of the flanges, tends to separate the bolted flanges, this gasket assembly must be firmly held in place by some proper means. In the original design [6], a large threaded plug was used, as shown in Figure 7.
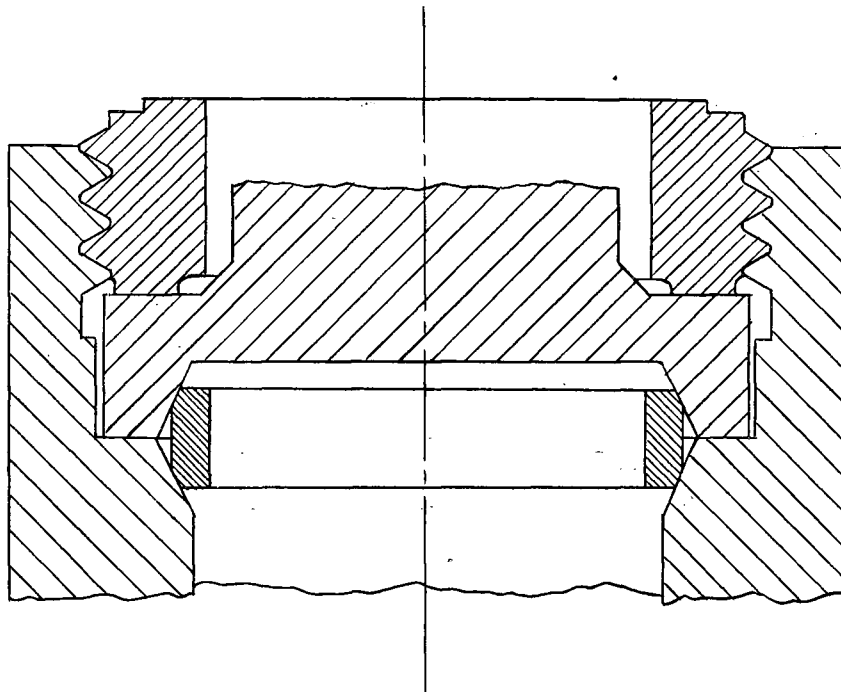
FIGURE 7 A Double-Cone Ring Gasket Assembly Utilizing Threaded Plug

This arrangement is satisfactory from the strength standpoint, but the threads are subjected to damage. It was then decided that large-diameter studs be adopted as the bolting devices.

In some modern designs, the double-cone type ring gasket is modified by cutting grooves on the seating bevels to reduce the contact area. An even more complicated modification has also been used in other heavy-duty applications, [5][6]. This modification, which is schematically shown in Figure 8, consists of providing a mechanical-backing shoulder to
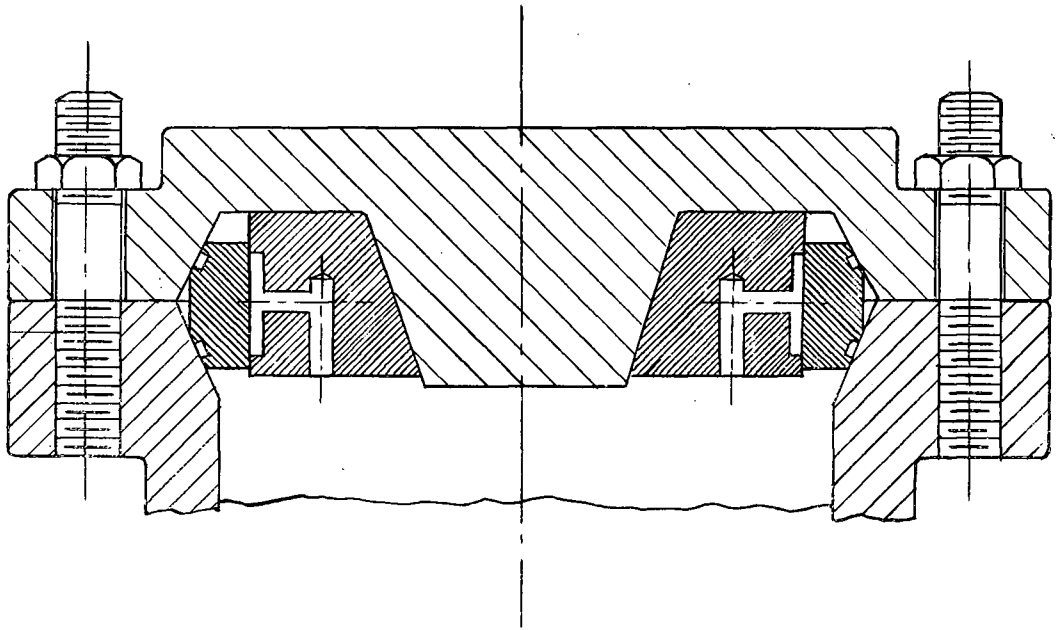
FIGURE 8 - A Modified Double-Cone Ring Gasket Design

prevent the ring from excessive inward deflection if it becomes necessary to preload the studs tighter than normal to overcome surface variation in gasket or flanges. A groove is cut in this shoulder for its entire circumference and holes provided to make certain that the applied hydrostatic pressure will act on the inner surface of the ring. However, for the sake of easy fabrication, these modifications were not applied to the ring models used in this investigation. The ring models remained as

plain-bevel, non-backing type.

CHAPTER III

THEORETICAL ANALYSIS

3.1 General

The elastic behaviour of the double-cone ring gasket used as a static seal may be theoretically analyzed in the sense that a longitudinal sliver $2b \cdot rd\emptyset \cdot h$ isolated from the ring gasket, as shown in Figure 9, can be treated as "a beam on elastic foundation".
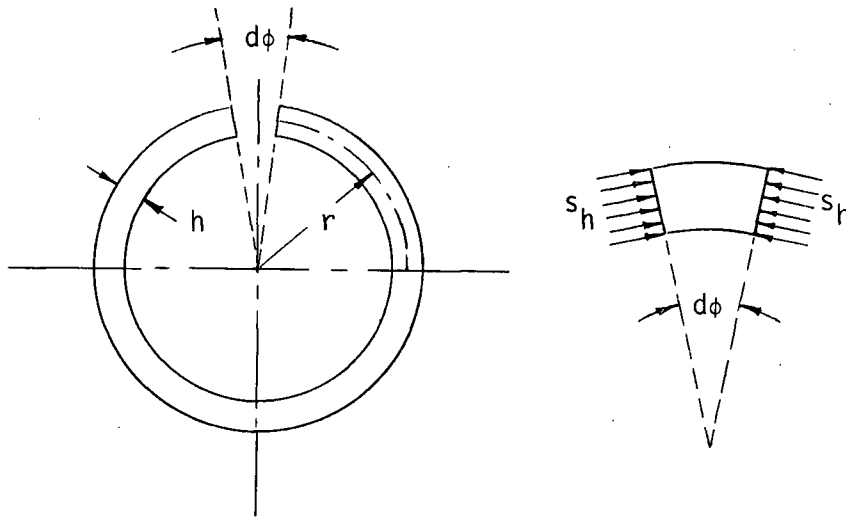
FIGURE 9   A Longitudinal Sliver Isolated from a Ring Gasket

If $rd\emptyset$ is taken to be unity, then the ring sliver becomes a beam of unit width, which rests on an elastic foundation consisting of the rest of the ring (covering an angle of $2\pi - d\emptyset$). This beam is acted upon by resultants of sealing pressure N, hydrostatic pressure p and hoop compressions s_h. The hoop compressions, which are assumed to be uniformly distributed along both sides of the ring sliver, are not quite in opposite directions, but include a small angle $d\emptyset$ between them. Therefore, the resultant of these hoop compressions, $s_h \cdot 2b \cdot h \cdot d\emptyset$, constitutes the

reaction force imposed on the "beam" by the "elastic foundation", and is proportional to the deflection of the beam.

3.2 Fundamental Assumptions

In developing the mathematical approach for analyzing the ring deformation under applied loads, some simplifying assumptions are to be made so that the resulting differential equation which governs the elastic line of a ring sliver is simplified to such an extent that it may be solved without too much mathematical difficulty. These assumptions are summarized as follows:

1) The material from which the ring is made is assumed to be homogeneous, isotropic and perfectly elastic.

2) The flanges between which the ring is assembled are assumed to be absolutely rigid, and the studs holding these flanges in place are assumed to have infinite strength, or, in other words, it is assumed that no flange deformation or stud stretch could occur.

3) A ring sliver is assumed to be a rectangular beam with uniform cross-sections, as shown in Figure 10. In addition, it is assumed that the beam equation may be used for a relatively small length-to depth ratio.

4) The resultant of the sealing pressure acting on each ring bevel can be resolved into two orthogonal components (see Figure 10). One of these components, $N\cos\theta$, which is in the radial direction of the ring, is assumed to act at the extreme outer edge of ring, while the other component $N\sin\theta$, also acting at the edge of the ring, is replaced by the statically equivalent

bending moment Nsinθ·h/2 and an axial force with a magnitude

equal to Nsinθ.
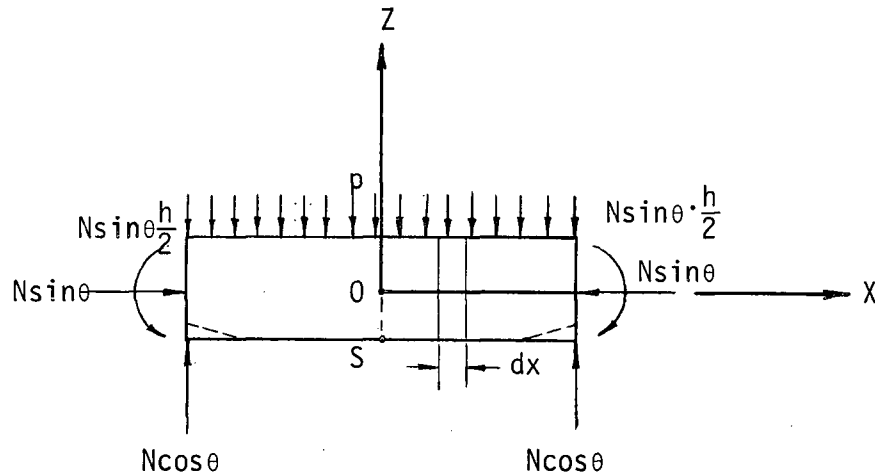
FIGURE 10 Simplified Boundary Conditions of a Ring Sliver

3.3 Derivation of the Governing Differential Equation

If a set of rectangular co-ordinate axes XYZ is chosen for the

beam (see Figure 10), an infinitesimal beam element dx is acted upon by shear

force V, bending moment M, hydrostatic pressure p and hoop compressions

s_h, as shown in Figure 11.
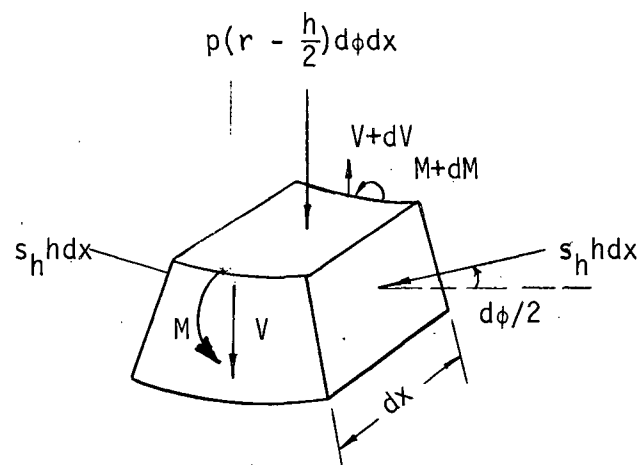
FIGURE 11 An Infinitesimal Beam Element

From the consideration of equilibrium of the forces acting on this beam element, it follows in the Z-direction

$$\frac{dV}{dx} = \frac{h}{r} s_h + p(1 - \frac{h}{2r}) \tag{3.1}$$

The magnitude of the hoop compression is given by the expression

$$s_h = E\frac{w}{r} - \mu \frac{(N\sin\theta + ph)}{h} \tag{3.2}$$

where E is Young's modulus, μ is Poisson's ratio and w is beam deflection in Z-direction consisting of the deflection attributable to bending, w_b, and that attributable to shear, w_s, i.e.

$$w = w_b + w_s$$

The bending moment in the beam is given by

$$M = -D \frac{d^2 w_b}{dx^2} \tag{3.3}$$

where D is the flexural rigidity

$$D = \frac{Eh^3}{12(1-\mu^2)}$$

The rate of change of the deflection due to shear [11] is given by

$$\frac{dw_s}{dx} = \frac{1.5V}{hG} = \frac{3(1+\mu)}{Eh} \cdot V \tag{3.4}$$

Combining Equations (3.1) to (3.4), and replacing $p(1 - \frac{h}{2r}) - \mu \frac{(N\sin\theta + ph)}{r}$ by $\bar{P}$, give

$$\frac{d^2 w}{dx^2} = -\frac{M}{D} + \frac{3(1+\mu)}{r^2} \cdot w + \frac{3(1+\mu)}{Eh} \cdot \bar{P} \tag{3.5}$$

Taking the derivative of (3.5) twice and using Equation (3.1) again, give

$$\frac{d^4w}{dx^4} - \frac{h^2}{1-\mu}\beta^4\frac{d^2w}{dx^2} + 4\beta^4w = -\frac{\bar{P}}{D} \qquad (3.6)$$

where

$$\beta^4 = \frac{3(1-\mu^2)}{h^2r^2}$$

This differential equation expresses the relation between the ring deformation and the applied loads, and is coincident with that derived by S. Levy for short cylindrical shells [12] allowing for reverse in sign of w.

3.4 Solution to the Governing Differential Equation

Any solution to the governing differential equation obtained in the preceeding section applies only to a particular ring gasket of mean radius r and thickness h. To overcome this and reduce the number of independent variables at the same time, Equation (3.6) is made dimensionless. This is done by defining two dimensionless parameters

$$\xi = \frac{x}{b} \qquad (3.7a)$$

and

$$\omega = \frac{w}{r} \qquad (3.7b)$$

Combining Equation (3.6) with Equations (3.7), and recalling that

$$\rho = \frac{r}{h} \text{ and } \alpha = \frac{b}{h}$$

as defined in last chapter give a dimensionless expression

$$\frac{d^4\omega}{d\xi^4} - \frac{3(1+\mu)\alpha^2}{\rho^2}\frac{d^2\omega}{d\xi^2} + \frac{12(1-\mu^2)\alpha^4}{\rho^2}\cdot\omega = -\frac{12(1-\mu^2)\alpha^4}{E\rho}\cdot\bar{P} \qquad (3.8)$$

The solution of Equation (3.8) with $\mu = 0.3$ is

$$\omega = C_1 \cosh \lambda\xi \cos \gamma\xi + C_2 \sinh \lambda\xi \sin \gamma\xi + C_3 \cosh \lambda\xi \sin \gamma\xi$$

$$+ C_4 \sinh \lambda\xi \cos \gamma\xi - P* \qquad (3.9)$$

in which, $P*$ is the particular integral

$$P* = \frac{\rho}{E} \bar{P} \qquad (3.10)$$

and, λ and γ are parameters defined for simplicity

$$\lambda = 1.285 \frac{\alpha}{\rho} \sqrt{\rho + .5901}$$

$$\gamma = 1.285 \frac{\alpha}{\rho} \sqrt{\rho - .5901}$$

and C_1, C_2, C_3, C_4 are constants of integration.

Since the deflection, w, is symmetrical with respect to the Z-axis

$$C_3 = C_4 = 0 \qquad (3.11)$$

Other boundary conditions useful in evaluating the non-zero constants C_1 and C_2 are:

1) The end displacement of beam, w_e, is a known quantity.

2) The bending moment at the ends of beam, $N\sin\theta \cdot \frac{h}{2}$ is known.

These two end conditions can be expressed mathematically as

$$\omega\Big|_{\xi=\pm 1} = \frac{w_e}{r} \qquad (3.12)$$

and

$$\left| \frac{d^2\omega}{d\xi^2} - \frac{3.9\alpha^2}{\rho^2} \omega - \frac{3.9\alpha^2}{\rho^2} p* \right|_{\xi=\pm 1} = - \frac{5.46\alpha^2 N\sin\theta}{E\rho h} \qquad (3.13)$$

respectively.

For simplicity, define

$$c_e = \frac{w_e}{r} \qquad (3.14)$$

and

$$M* = - \frac{5.46\alpha^2 N\sin\theta}{E\rho h} \tag{3.15}$$

Then the end conditions (3.12) and (3.13) become

$$\omega\Big|_{\xi=\pm 1} = c_e \tag{3.16}$$

and

$$\left|\frac{d^2\omega}{d\xi^2} - \frac{3.9\alpha^2}{\rho^2}\omega - \frac{3.9\alpha^2}{\rho^2}P*\right|_{\xi=\pm 1} = M* \tag{3.17}$$

Substituting Equation (3.9) into (3.16) and (3.17) and solving
the resulting simultaneous equations, yield

$$C_1 = \frac{1}{2\lambda\gamma(\sinh^2\lambda + \cos^2\gamma)}$$

$$\{(C_e + P*)[2\lambda\gamma\cosh\lambda\cos\gamma + (\lambda^2 - \gamma^2 - 3.9\alpha^2/\rho^2)\sinh\lambda\sin\gamma]$$

$$- M*\sinh\lambda\sin\gamma\} \tag{3.18}$$

and

$$C_2 = \frac{1}{2\lambda\gamma(\sinh^2\lambda + \cos^2\gamma)}$$

$$\{(c_e + P*)[2\lambda\gamma\sinh\lambda\sin\gamma - (\lambda^2 - \gamma^2 - 3.9\alpha^2/\rho^2)\cosh\lambda\cos\gamma]$$

$$+ M*\cosh\lambda\cos\gamma\} \tag{3.19}$$

At this point, it is recognized that to combine Equation (3.9)
with Equations (3.10), (3.18) and (3.19) does not give the complete
solution to the deflection, because there is still an unknown quantity,
N, involved in P* and M*. However, this can be clarified by noting
another boundary condition that

$$\frac{dM}{dx}\Big|_{x=+b} = N\cos\theta \tag{3.20a}$$

or, in alternate form

$$\left| \frac{d^3\omega}{d\xi^3} - \frac{3.9\alpha^2}{\rho^2} \frac{d\omega}{d\xi} \right|_{\xi=+1} = - \frac{10.92\alpha^3 \cos\theta}{\rho} \left(\frac{N}{Eh}\right) \qquad \text{(3.20b)}$$

After some cumbersome operations, the expression for the magnitude of sealing force per unit length of ring circumference, N, can be obtained by solving the following equation

$$\frac{N}{Eh} = K_c \cdot c_e + K_p \cdot \frac{p}{E} \qquad \text{(3.21)}$$

in which K_c and K_p are coefficients relating c_e and $\frac{p}{E}$ to the quantity $\left(\frac{N}{Eh}\right)$

$$K_c = \frac{1}{\text{Den.}} [(2\lambda^2\gamma\Gamma_1 - \gamma\Gamma_0\Gamma_2)\cosh\lambda \sinh\lambda$$

$$- (2\lambda\gamma^2\Gamma_2 + \lambda\Gamma_0\Gamma_1) \cos\gamma \sin\gamma]$$

and

$$K_p = \frac{1}{\text{Den.}} (\rho-0.8)[(2\lambda^2\gamma\Gamma_1 - \gamma\Gamma_0\Gamma_2)\cosh\lambda \sinh\lambda$$

$$- (2\lambda\gamma^2\Gamma_2 + \lambda\Gamma_0\Gamma_1)\cos\gamma \sin\gamma]$$

where Γ_0, Γ_1, Γ_2 and Den. are defined for simplicity

$$\Gamma_0 = \lambda^2 - \gamma^2 - 3.9\alpha^2/\rho^2$$

$$\Gamma_1 = \lambda^2 - 3\gamma^2 - 3.9\alpha^2/\rho^2$$

$$\Gamma_2 = 3\lambda^2 - \gamma^2 - 3.9\alpha^2/\rho^2$$

and

$$\text{Den.} = 0.3 \sin\theta [2\lambda^2\gamma\Gamma_1 - \gamma\Gamma_0\Gamma_2 + 18.2(\alpha^2/\rho)\Gamma_2]\cosh\lambda \sinh\lambda$$

$$- 0.3 \sin [2\lambda\gamma^2\Gamma_2 + \lambda\Gamma_0\Gamma_1 - 18.2(\alpha^2/\rho)\Gamma_1]\cos\gamma \sin\gamma$$

$$- 21.84(\alpha^3/\rho)\lambda\gamma\cos\theta(\sinh^2\lambda + \cos^2\gamma)$$

Then, Equations (3.18), (3.19) and (3.10) reduce to

$$C_1 = \frac{c_e}{2\lambda\gamma(\sinh^2\lambda + \cos^2\gamma)}$$

$$\{[\Gamma_0 - 0.3(\Gamma_0 - 18.2\alpha^2/\rho)\sin\theta \cdot K_c]\sinh\lambda\sin\gamma$$

$$+ 2\lambda\gamma(1 - 0.3\sin\theta \cdot K_p)\cosh\lambda\cos\gamma\}$$

$$+ \frac{p/E}{2\lambda\gamma(\sinh^2\lambda + \cos^2\gamma)}$$

$$\{[(\rho - 0.8)\Gamma_0 - 0.3(\Gamma_0 - 18.2\alpha^2/\rho)\sin\theta \cdot K_p]\sinh\lambda\sin\gamma$$

$$+ 2\lambda\gamma[(\rho - 0.8) - 0.3\sin\theta \cdot K_p]\cosh\lambda\cos\gamma\} \qquad (3.22)$$

$$C_2 = \frac{c_e}{2\lambda\gamma(\sinh^2\lambda + \cos^2\gamma)}$$

$$\{2\lambda\gamma(1 - 0.3\sin\theta \cdot K_c)\sinh\lambda\sin\gamma$$

$$-[\Gamma_0 - 0.3(\Gamma_0 - 18.2\alpha^2/\rho)\sin\theta \cdot K_c]\cosh\lambda\cos\gamma\}$$

$$+ \frac{p/E}{2\lambda\gamma(\sinh^2\lambda + \cos^2\gamma)}$$

$$\{2\lambda\gamma[(\rho - 0.8) - 0.3\sin\theta \cdot K_p]\sinh\lambda\sin\gamma$$

$$-[(\rho - 0.8)\Gamma_0 - 0.3(\Gamma_0 - 18.2\alpha^2/\rho)\sin\theta \cdot K_p]\cosh\lambda\cos\gamma\}$$

$$(3.23)$$

and

$$P^* = -0.3\sin\theta \cdot K_c \cdot c_e + [(\rho - 0.8) - 0.3\sin\theta \cdot K_p] \cdot \frac{P}{E} \qquad (3.24)$$

Substituting these values into Equation (3.9) gives the final solution to the differential equation (3.8). This solution in turn indicates the radial deflection of the ring.

In particular, at the center of the ring sliver concerned, i.e. at the origin of the co-ordinate system chosen, where

$$x = 0, \quad \text{or } \xi = 0$$

the solution reduces to

$$\omega_{\xi=0} = \omega_0 = C_1 - P^* \qquad (3.25)$$

3.5 Tangential Strains of Ring Gasket

Since the double-cone ring gasket is axisymmetrical in geometry and is subjected to axisymmetrical loading, the tangential strain at the centroid of any axial cross-section of the ring gasket is

$$\varepsilon_0 = -\frac{w_0}{r} = -\omega_0 \qquad (3.26)$$

the minus sign in the right-hand side denotes that an inward deflection gives a compressive strain.

Furthermore, the tangential strain at the point S (see Figure 10), which is on the outer surface of the ring gasket, is given as

$$\varepsilon_s = \varepsilon_0 + \frac{\mu(N\sin\theta + ph)}{Eh}$$

$$= \varepsilon_0 + 0.3 K_c \sin\theta \cdot c_e + K_p(1 + \sin\theta) \cdot \frac{p}{E} \qquad (3.27)$$

Equation (3.27) is of practical interest because in the experimental part of this investigation, the tangential strains at point S were actually measured by using strain gages.

3.6 Effects of Design Parameters on Ring Deformation and Sealing Pressure

The combination of Equation (3.26) with Equations (3.25), (3.22) and (3.24) gives an alternate expression for the tangential strain at the centroid of any axial cross-section of ring

$$\varepsilon_0 = -\eta_c \cdot c_e + \eta_p \cdot \left(\frac{p}{E}\right) \qquad (3.28)$$

where

$$\eta_c = \frac{1}{2\lambda\gamma(\sinh^2 + \cos^2)}$$

$$\{[\Gamma_0 - 0.3(\Gamma_0 - 18.2\alpha^2/\rho)\sin\theta \cdot K_c]\sinh\lambda\sin\gamma$$

$$+ 2\lambda\gamma(1 - 0.3\sin\theta \cdot K_p)\cosh\lambda\cos\gamma\} + 0.3K_c\sin\theta \qquad (3.29)$$

and

$$\eta_p = \frac{-1}{2\lambda\gamma(\sinh^2\lambda + \cos^2\gamma)}$$

$$\{[(\rho - 0.8)\Gamma_0 - 0.3(\Gamma_0 - 18.2\alpha^2/\rho)\sin\theta \cdot K_p]\sinh\lambda\sin\gamma$$

$$+ 2\lambda\gamma[(\rho - 0.8) - 0.3\sin\theta \cdot K_p]\cosh\lambda\cos\gamma\}$$

$$+ (\rho - 0.8) - 0.3K_p\sin\theta \qquad (3.30)$$

are coefficients relating c_e and $\frac{p}{E}$ to the tangential strain of ring respectively. By using a digital computer for rapid calculations, the relationships between these two coefficients and the design parameters of ring, as well as the relationships between coefficients, K_c and K_p (see Equation (3.21)), and the design parameters, are shown in Figures 12 to 15. From these figures, the effects of the design parameters, ρ and α, on the ring deformation and the sealing force can be readily seen.

FIGURE 12 Relationship Between K_c and Design Parameters, α and ρ, for Double-Cone Ring Gaskets with $\theta=12.5°$

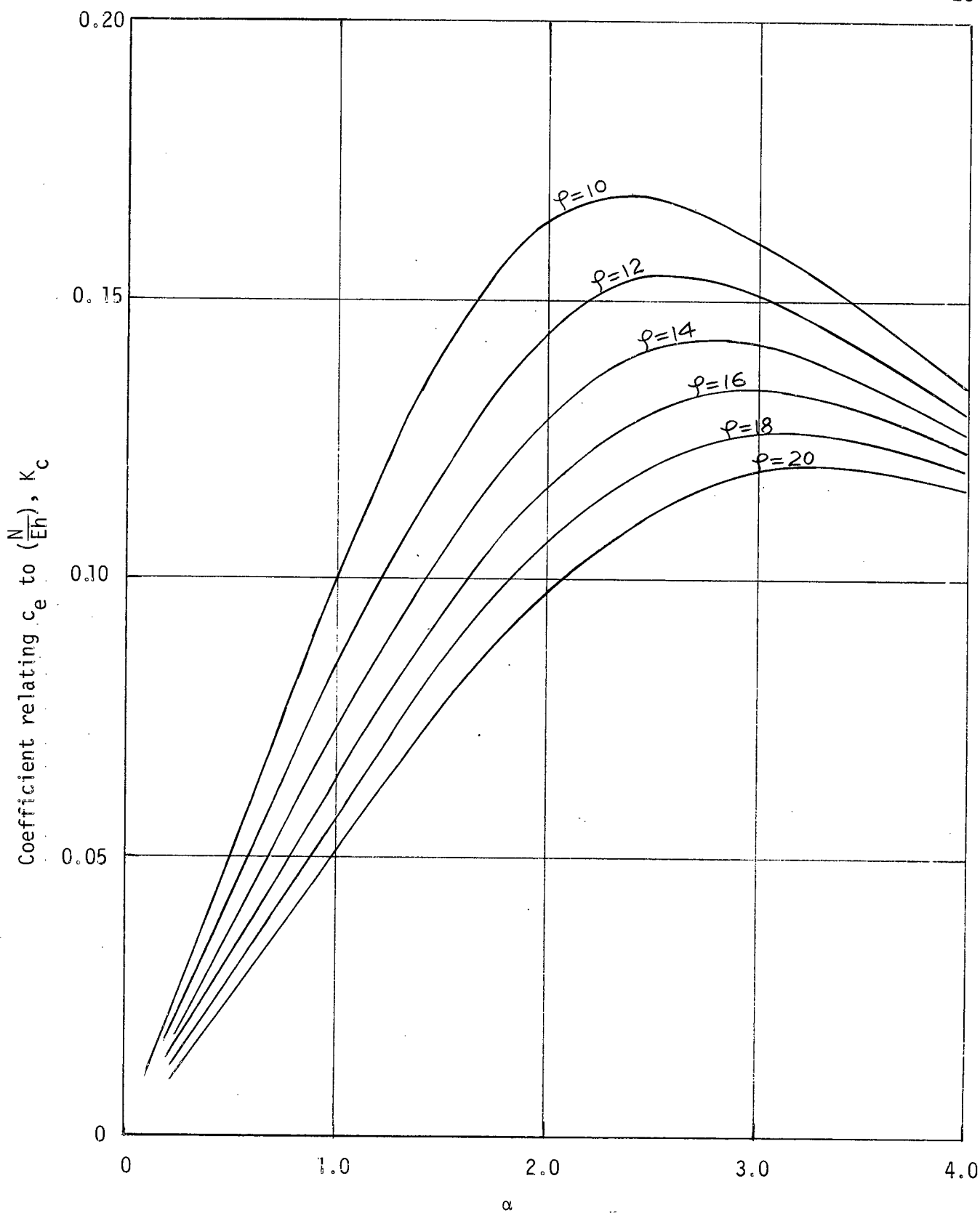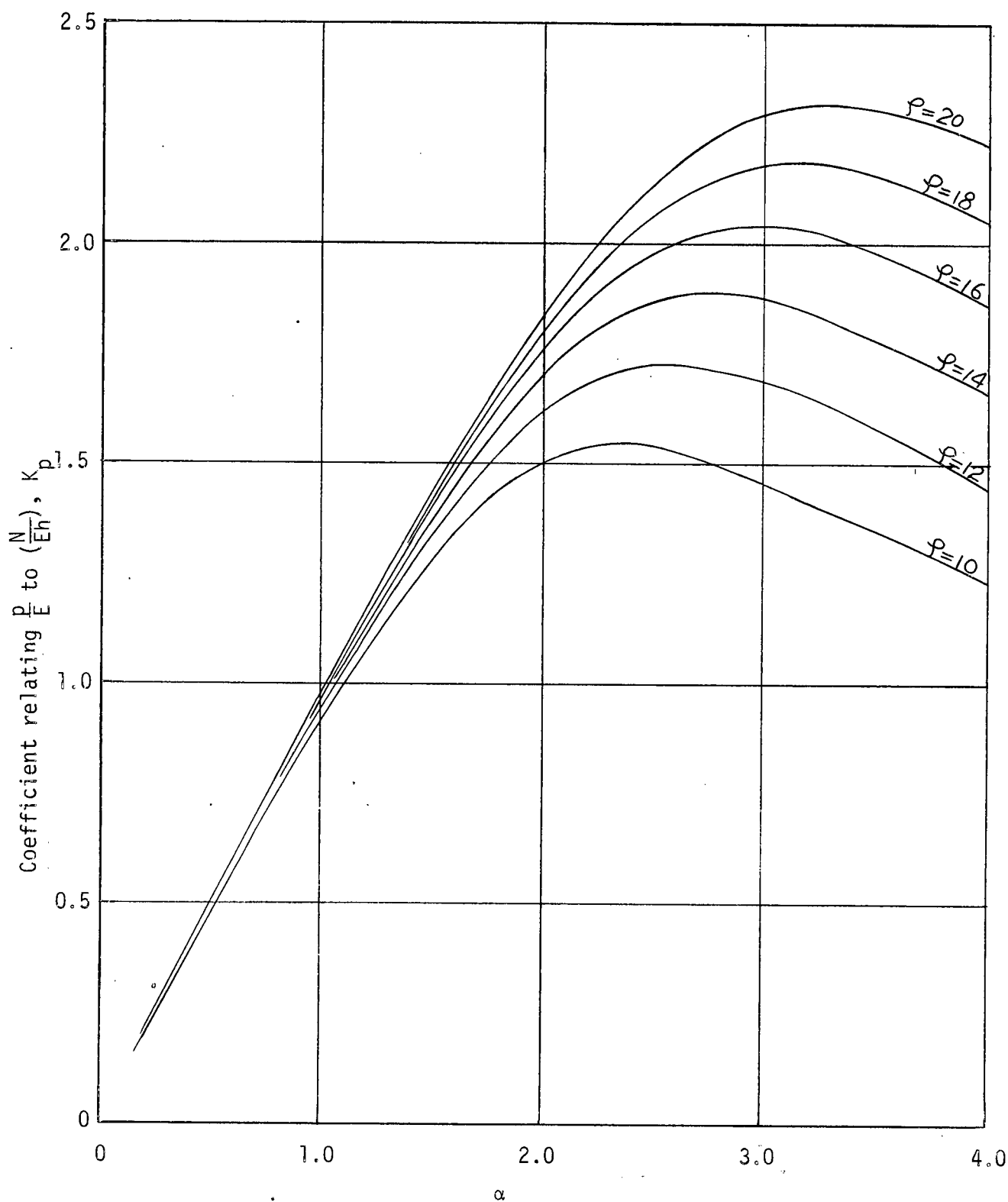FIGURE 13 Relationship Between K_p and Design Parameters, α and ρ, for Double-Cone Ring Gaskets with $\theta = 12.5°$
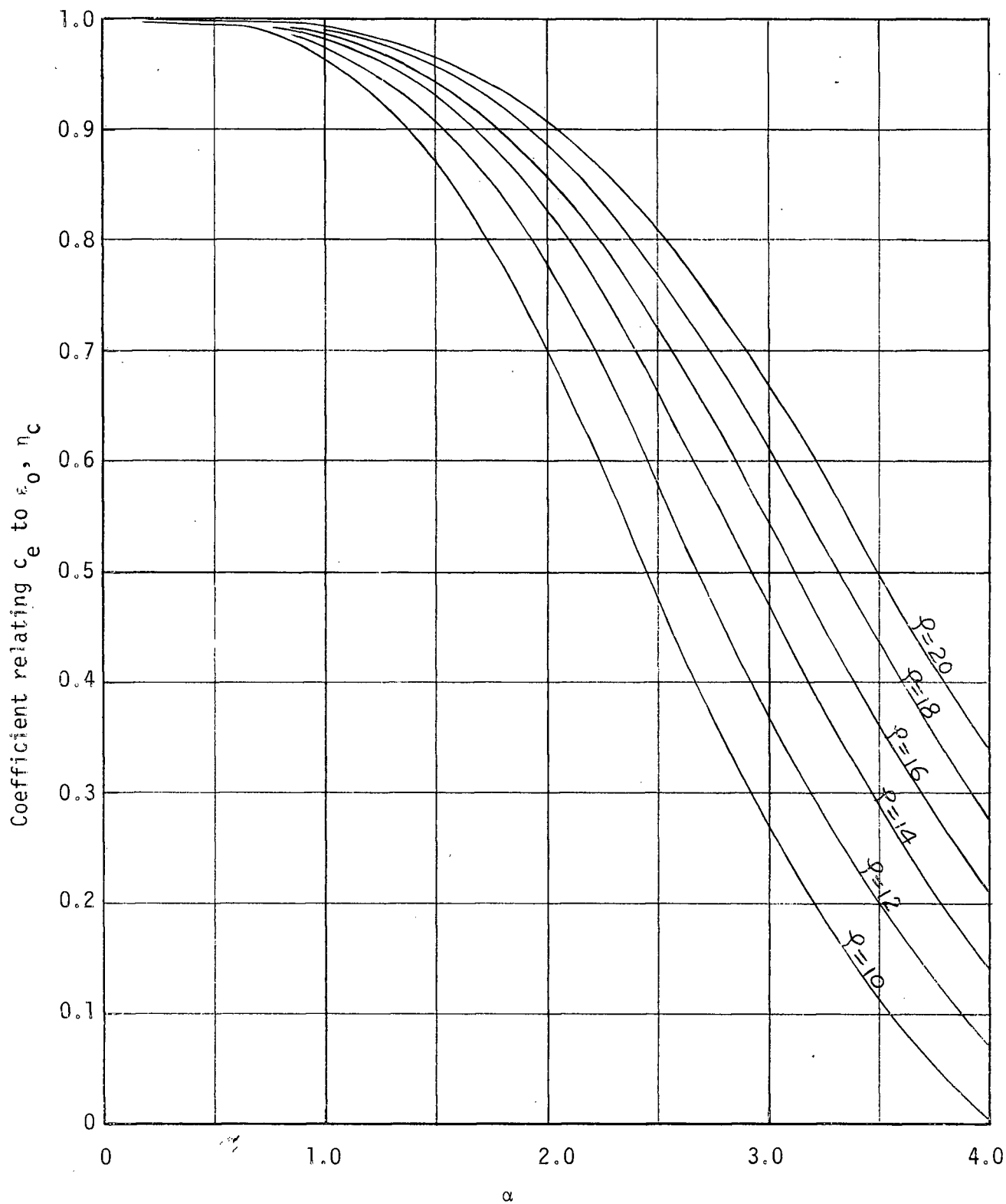
FIGURE 14 Relationship Between η_c and Design Parameters, α and ρ, for Double-Cone Ring Gaskets with $\theta=12.5°$
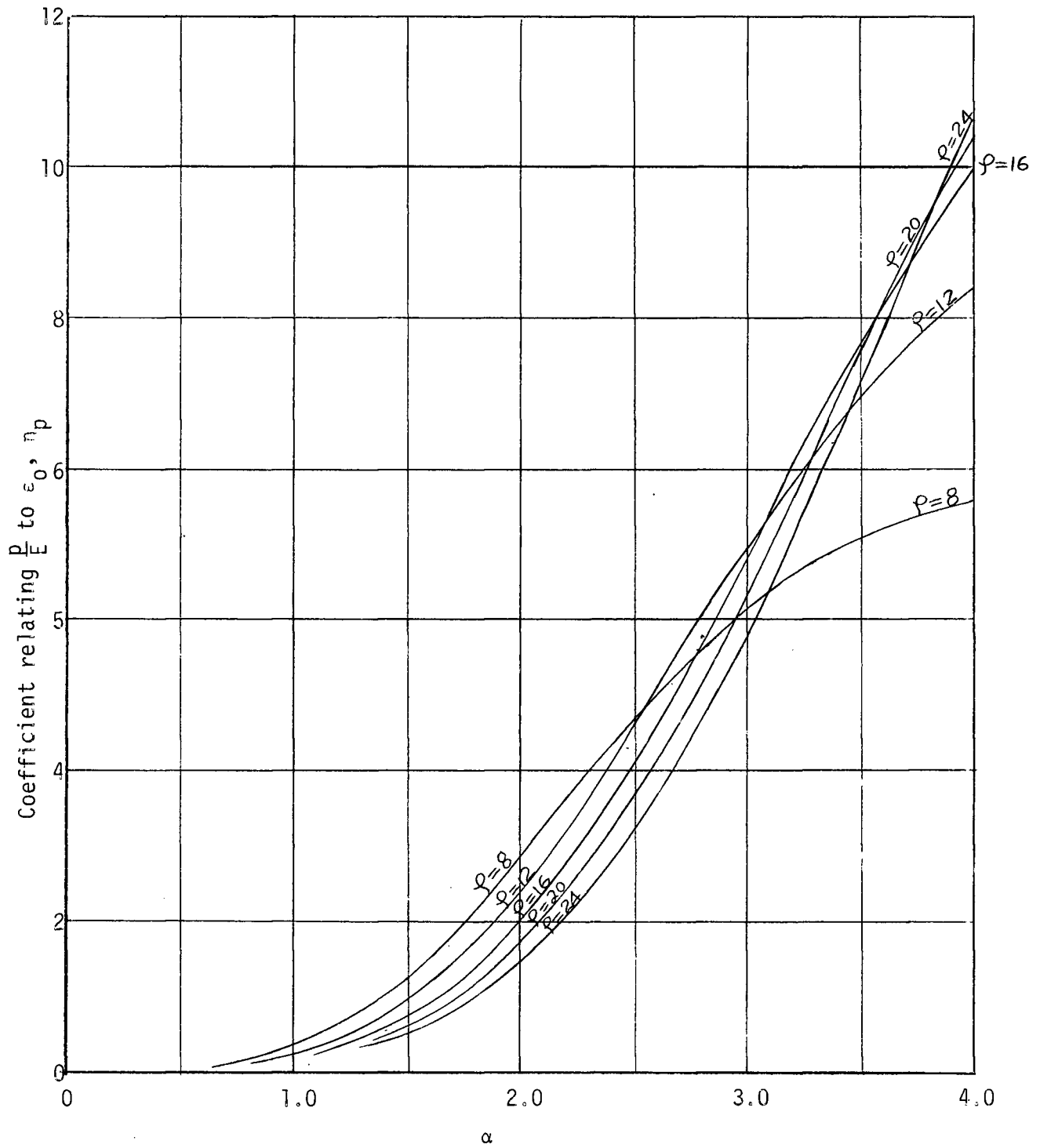
FIGURE 15 Relationship Between η_p and Design Parameters, α and ρ, for Double-Cone Ring Gaskets with $\theta=12.5°$

CHAPTER IV

DESCRIPTION OF TEST MODELS

4.1 Model Material

All of the ring models used in this investigation were fabricated
from SAE 1020 carbon steel. As received, the model material appeared in the
form of round, seamless, cold-drawn tubing which was supplied by the
Wilkinson Company, Limited. The tubing was 6 1/4 in. in outside diameter and
1/2 in. thickness, without any heat-treatment when purchased.

In fabricating the ring models, sections with suitable lengths
were cut from the tubing. Some of these tubing sections in as-received
condition were then turned on a lathe to the predetermined shapes, and
the resultant rings were designated Models A1, B1, B2, C1 and C2 according
to their dimensions, as outlined in next section. As for Models A2, B3
and C3, the fabrication process was somewhat different from that just
described. The associated tubing sections were softened by annealing
before machining operations. The annealing temperature was 1350° F.

Since the physical properties of the cold-drawn tubing depend
upon the degree of cold work performed in producing each piece, tension
tests were performed to secure reliable information about the proportional
limits and the ultimate strengths of the model materials, which were of
the most importance for analyzing the behaviour of the ring models.

In performing the tension tests, test specimens were cut from
the cold-drawn and the annealed tubing sections, and then loaded to
failure in an Instron testing machine. Table 1 shows the results of the
tension tests, along with the average Rockwell readings of the model
materials as taken from the hardness tests.

TABLE 1

Physical Properties of Model Materials

MATERIAL	PROPORTIONAL LIMIT	ULTIMATE STRENGTH	ELONGATION IN 2 IN.	ROCKWELL B.
Cold-drawn	52,000 psi.	87,000 psi.	14%	94
Annealed	33,000 psi.	57,000 psi.	38%	70

4.2 Design Details of Ring Models

In designing a ring model, suitable numerical values were first selected for the design parameters α and ρ, as well as the pressure-contact ratio k. Then, the ratio of the radial component of end displacement of the ring in the assempled state to its mean radius, c_0, was predetermined by considering the required initial sealing pressure. This ratio was given by the following expression:

$$c_0 = \frac{g \cdot \tan\theta}{2r} \tag{4.1}$$

in which g was the initial stand-off of the flanges with the ring snugly located between them, and θ was the inclination angle of the seating bevels of the ring, which, in this investigation, was taken as 12.5 degress.

With all of these predetermined values chosen, the thickness of the ring model was then calculated from the geometrical relation

$$h = \frac{R}{(1 - c_0)\rho + (1 - 1/k)\alpha\tan\theta + .5} \tag{4.2}$$

where R was the maximum radius of the bore of flanges, which was also a fixed quantity of 3 in. in the present investigation.

In order to observe the effect on the performance of the ring gasket as the proportions between the ring dimensions were changed,

eight ring models were designed, each with different dimensions. According
to their α-values, these eight models were divided into three groups,
namely, the wide-ring, the mid-ring and the narrow-ring series. Table 2
shows the design parameters of the ring models, along with their nominal
dimensions.

4.3 Preparation of Test Model

Because of their stability, accuracy and relatively small sizes,
the bonded, variable-resistance-strain gages had been generally accepted
as one of the best strain-sensing devices for experimental stress
analysis, and thus adopted in this investigation to measure the deformations
of the ring models in working condition.

The strain gages used were of the Budd C6-141-B type, with the
following characteristics:

Gage Factor: 2.05 ± 1/2%

Gage Resistance: 120 ± .2 ohms

Gage Length: 1/4 in.

Grid Form: Etched Metalfilm

In preparing for tests, the strain gages were bonded to the ring
models with GA-2 polymeric cement which was also supplied by the Budd
Company. The bonding procedure was performed following the recommendations
of the supplier.

In order to measure both axial and tangential strains of the
ring, for each model of the wide-ring series, four two-element rectangular
gage-rosettes were applied to the ring and were equally spaced around its
outside circumference. However, for other ring models, due to their
limited widths, only four single strain gages oriented in the tangential
direction were applied to each ring. The photograph in Figure 16 shows
both kinds of gage-arrangement.

TABLE 2

Design Parameters and Dimensions of Test Models

SERIES	MODEL NO.	DESIGN PARAMETERS		PRESSURE- CONTACT RATIO	OUTSIDE DIA. IN.	INSIDE DIA. IN.	WIDTH IN.	THICK- NESS IN.	REMARKS
		α	ρ						
wide-ring	A1	3	15	3	5.8590	5.4810	1.1340	.1890	cold-drawn
	A2	3	15	6	5.8094	5.4346	1.1244	.1874	annealed
mid-ring	B1	2	15	3	5.8900	5.5100	.7600	.1900	cold-drawn
	B2	2	15	3	5.9086	5.5274	.7624	.1906	cold-drawn
	B3	2	15	6	5.8776	5.4984	.7584	.1896	annealed
narrow-ring	C1	1	10	6	5.9325	5.3675	.5650	.2825	cold-drawn
	C2	1	12	6	5.9354	5.4606	.4748	.2374	cold-drawn
	C3	1	12	6	5.9225	5.4487	.4738	.2369	annealed
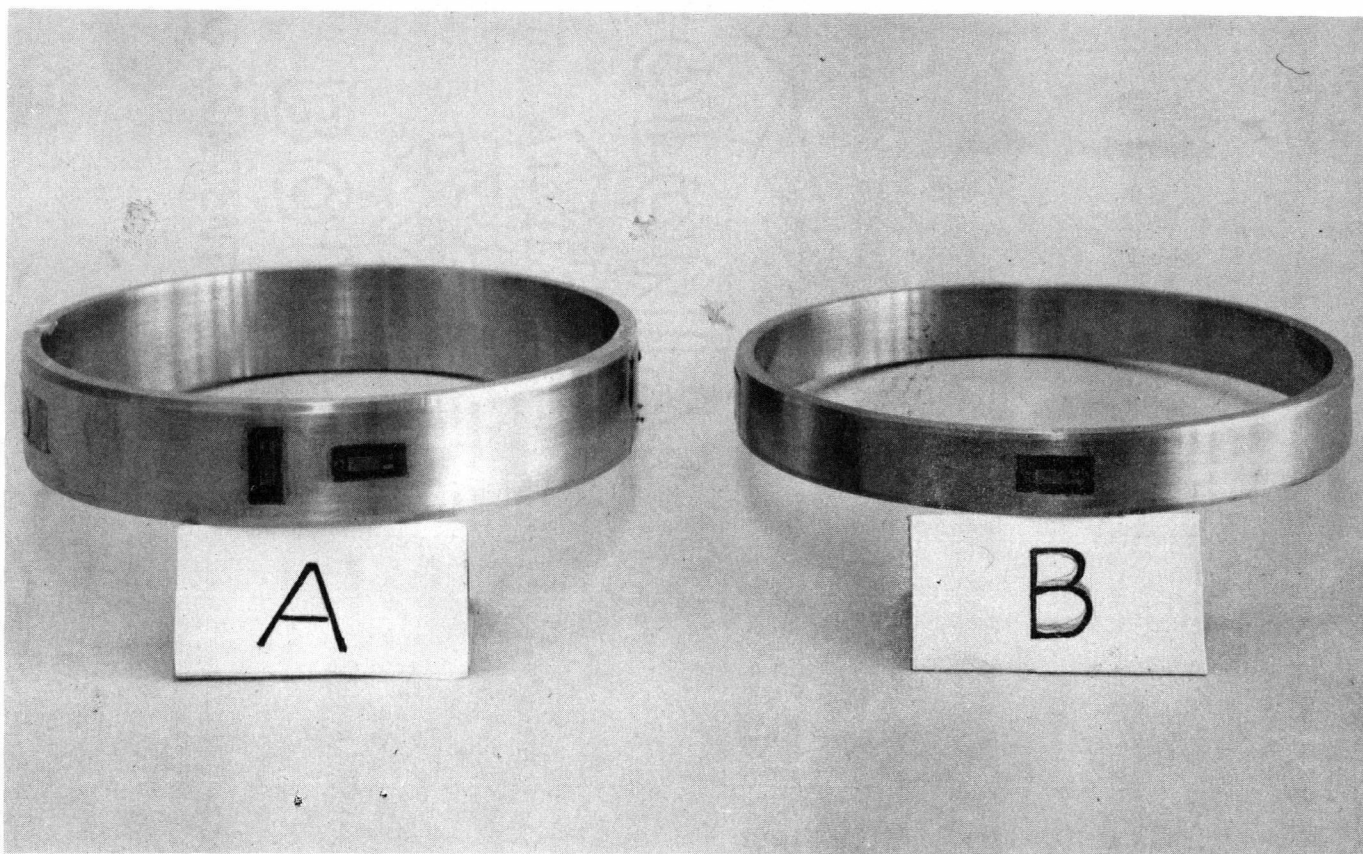
FIGURE 16 Gage-Arrangements for (a) A Wide-Ring Model, and (b) A Mid-Ring Model

To provide the means of communicating the signals from a strain gage to the strain-indicating device during the ring model tests, electrical lead was soldered to the gage subsequently to the curing of the bonding material. Usually, the lead used in this investigation was of the three-wire type for the reason that the changes in lead-wire resistance due to the temperature changes of a three-wire lead could be made self-compensating.

CHAPTER V

INSTRUMENTATION AND TEST PROCEDURE

5.1 Description of Apparatus

The apparatus used for testing the ring models is shown in the photograph in Figure 17. This apparatus consists of the following components:

Pressure Chamber

SPS 245 steel was chosen for fabricating the pressure chamber because of its high strength and rigidity. The chamber consisted of two major parts; the top cover and the vessel. Design details of these two parts of chamber are shown in Figures 18 and 19, and their general views are photographically presented in Figure 20.

For assembling the cover and the vessel together, twelve 3/4 in. studs were provided. These studs were firmly fastened on the vessel, as clearly shown in the photographic picture. Of these twelve studs, three were with a centre hole in which Budd-140-B strain gages were installed to measure the stud strains during the tests.

Hydraulic Pump

The choice of the pressure source in the testing system was greatly influenced by the ease with which the pressure applied to the pressure chamber could be controlled. From this point of view, an Enerpac P-85 hand pump manufactured by the Blackhawk Industrial Products Company was selected. This pump was a self-contained, piston-type hydraulic pump with a rated capacity of 10,000 psi.
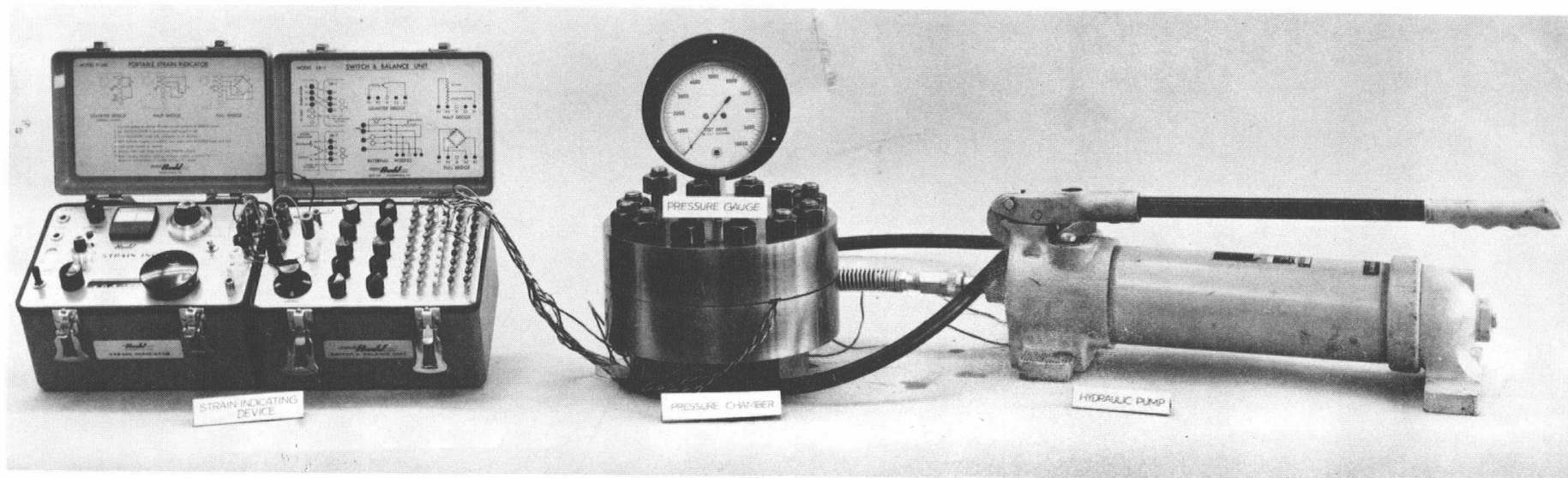
FIGURE 17   Arrangement of the Testing Apparatus

3/16 Drill,
12 Holes on
7-1/2 Bolt Cicrle

3/8-16 UNC Tap,
4 Holes on 7-1/2 Bolt Circle

7/16 Drill
1-3/4 Deep

$2\frac{1}{4}$

1/16 Deep x 1/2 Wide
4 Grooves
Equally
Spaced

27/64 Drill
1/4 Pipe Tap

$9\frac{1}{2}$

$6 \pm .001$

$\frac{3}{4}$

$\frac{1}{8}$ R

$12\frac{1}{2}°$

FIGURE 18   Design Details of the Top Cover

1/16 Deep x 1/2 Wide
4 Grooves
Equally Spaced

3/4-10 UNC Tap
12 Holes on
7-1/2 Bolt Circle

$2\frac{1}{4}$

$9\frac{1}{2}$

$6 \pm .00\frac{1}{16}$

$\frac{3}{4}$

$\frac{1}{8}$R

12.5°

27/64 Drill
1/4 Pipe Tap

FIGURE 19 Design Details of the Vessel

FIGURE 20 General Views of (a) The Top Cover, and (b) The Vessel

In order to form the union of the pump with the pressure chamber, a 3/8 in. flexible hose with plug-in type couplers was also supplied by the pump manufacturer. Through this hose, the hydraulic oil under pressure was transmitted from the pump to an inlet opening located at the bottom of the pressure chamber.

Pressure Gauge

The pressure gauge used in this investigation was supplied by the American Standard Advanced Technology Laboratories. It was a Bourdon spring-type gauge capable of indicating pressure up to 10,000 psi. and with a readability of 50 psi. In working, the pressure-sensing element of the gauge, which was essentially a tube flattened and bent to an arc of a circle, was exposed to the pressure in the pressure chamber through a bottom connection of the gauge, and then with a suitable multiplying mechanism, the intensity of pressure was shown by the position of a pointer on the gauge dial.
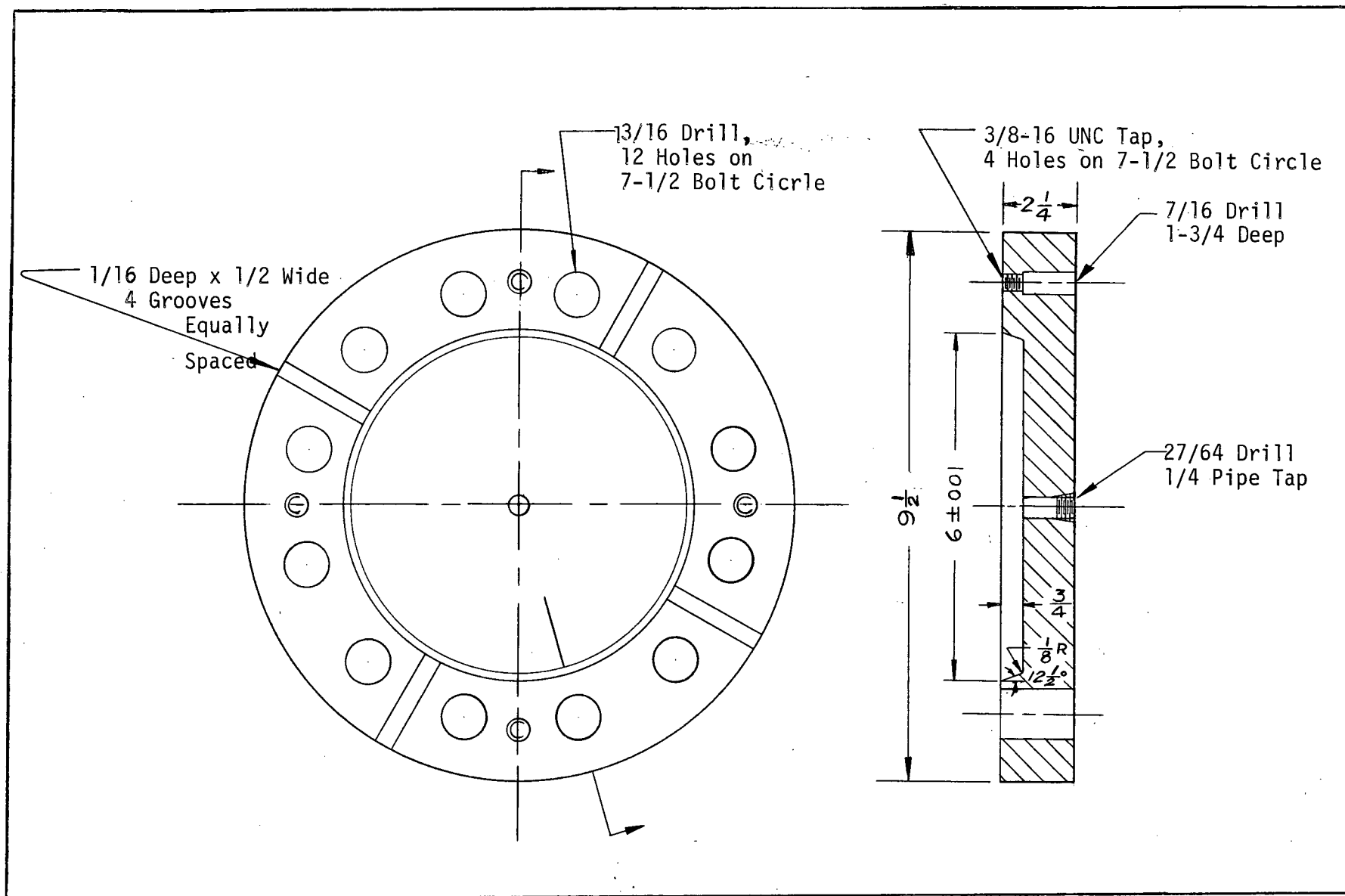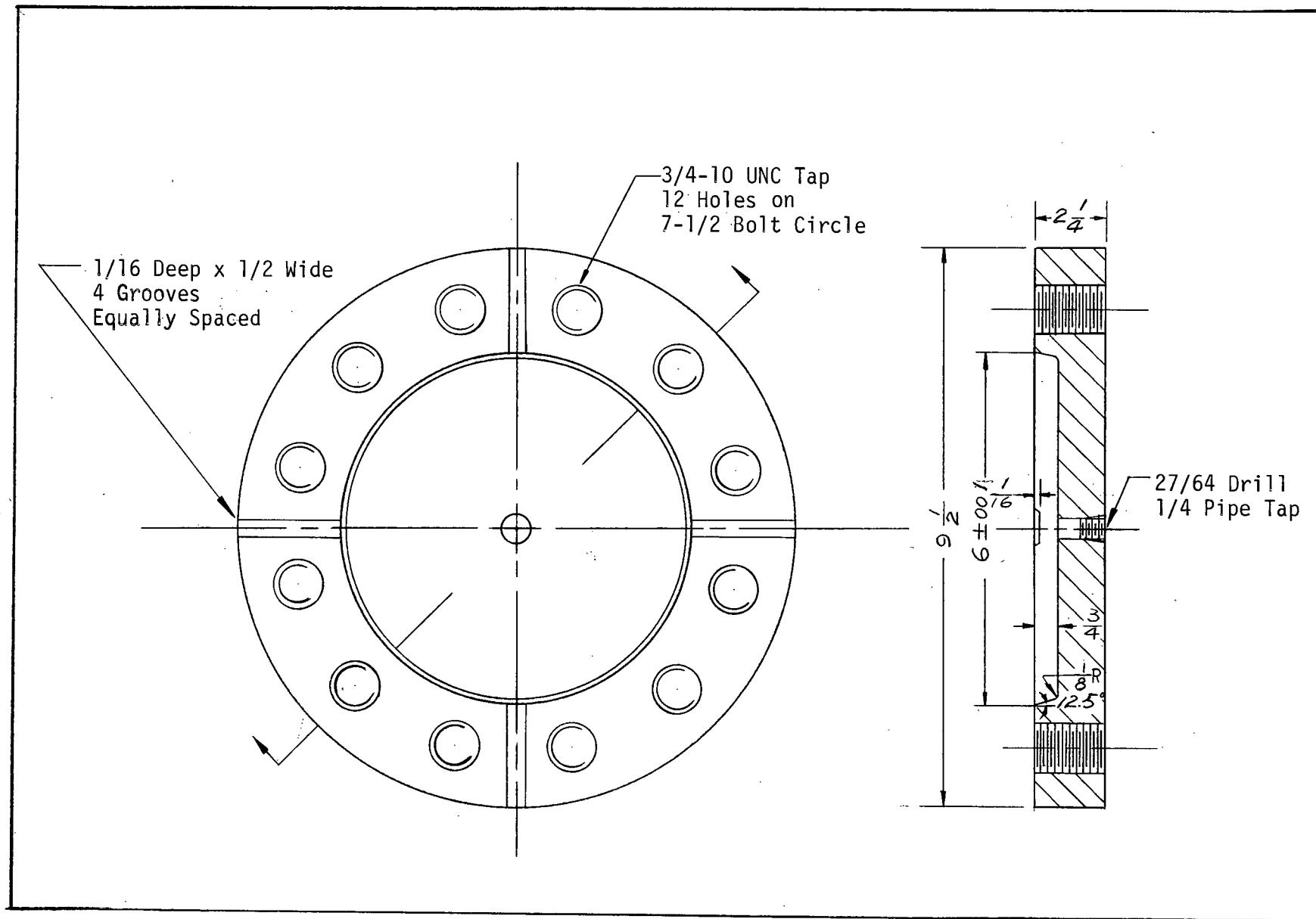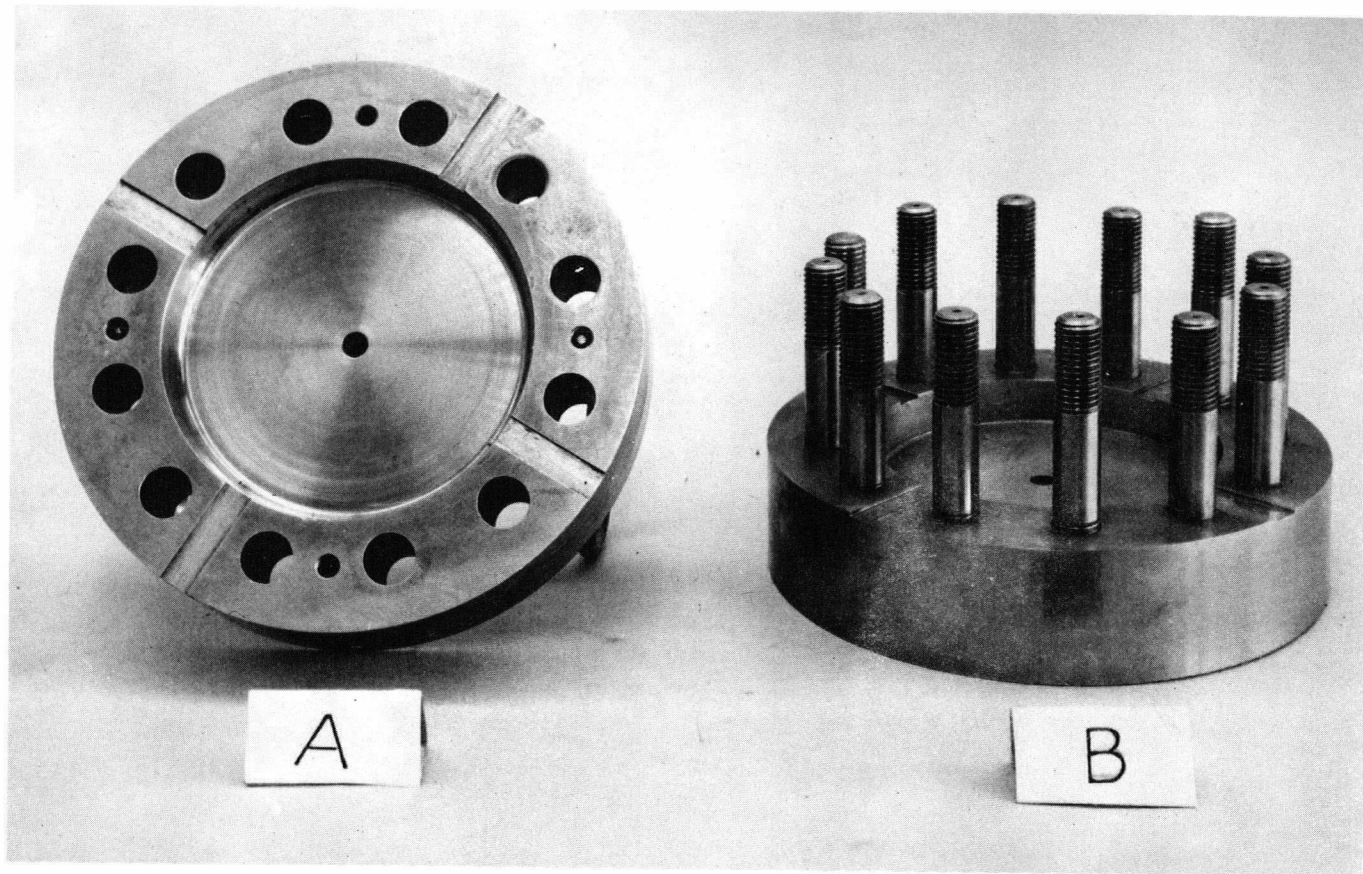
Strain-Indicating Device

The strain-indicating device used consisted mainly of a P-350 Strain Indicator which was manufactured by the Instrument Division of the Budd Company. This instrument was designed primarily for use in determining static strains when used with resistance-type strain gages, and with the following characteristic features:

Range: ±50,000 µ strains

Accuracy: ±5 µ strains or ±5%

Readability: 1 µ strain

Sensitivity: 40 - 2,000 µ strains for full scale one side meter deflection

External Circuits: full, half or quarter-circuit

Internal Dummies: 120 and 350 ohms

Battery: 9 volts

Amplifier: A-C transistorized.

This indicator was also equipped with a control for adjusting circuit balance and a selector for switching the internal dummy half-bridge into external circuit for quarter- and half-bridge applications. In this investigation, only the quarter-bridge external circuit, as shown in Figure 21, was employed.
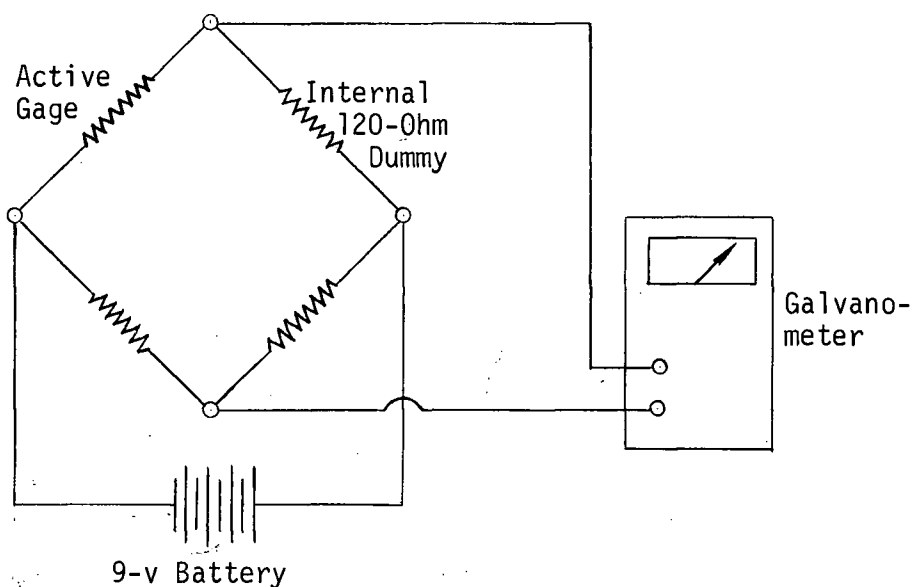
FIGURE 21 External Quarter-Bridge Circuit with Internal Dummy

Another major component of the strain-indicating device was a Budd SB-1 Switch and Balance Unit. By combining this Switch and Balance Unit with the Strain Indicator just described, a strain-measuring operation to read gage points up to a number of 10 was possible.

5.2 Test Procedure

The procedure of testing a ring model could be divided in two distinct parts; one in which the ring model was assembled into a proper

position in the pressure chamber, and in the other the hydrostatic pressure was applied to the ring. These two parts of a ring-model test were denoted as the assembly and the pressure test respectively, and will be separately described in the remainder of this section.

Assembly

The method of assembling a ring model into the pressure chamber was as follows. With the ring bevels and the sealing surfaces of the pressure chamber coated with a thin layer of Rulon anti-stick agent, the ring model was placed into the pressure chamber, and snugly rested in a position between the top cover and the vessel of the chamber. At this point, the gap between the flange of the cover and that of the vessel was measured and recorded. This initial value of gap, g, could be checked with the one predetermined in the design of the ring model through the utilization of Equation (4.1). Then, after the strain gages on the ring model had been connected to the strain-indicating device, the top cover of the chamber was lowered by tightening the nuts on the studs until its flange came in contact with that of the vessel face to face and the assembly of the ring model was completed. During this assembly process, great care should be taken to obtain an even tightening of nuts for maintaining an uniform gasket loading and preventing the ring from shifting out of place. Usually, this was done by conducting the assembly process in a suitable number of steps. At each step, the gap of the pressure chamber was checked at four chosen points and the strain measurement of the ring was taken.

Pressure Test

The purpose of a pressure test was to observe the sealing capacity of the ring model being tested, and to measure the ring deformation due to

the applied hydrostatic pressure. In this test, the oil under pressure was transmitted from the hydraulic pump to the bolted chamber and acted on the assembled ring model. The intensity of pressure was increased from 0 to 10,000 psi. in ten increments, and strain measurement of the ring was taken at each increment. In addition, the tensile strain readings of the studs were also recorded in the test.

CHAPTER VI

EXPERIMENTAL RESULTS AND DISCUSSIONS

6.1 Results of Strain-Measurements

The strain-measurements made in testing the ring models determined the tangential strains on the outer surfaces of the models tested. This was based on the consideration that these strains not only gave an indication of the ring deformations during tests, but also provided a means to check the validity of the theoretically developed formulas.

During the tests, the strain-readings read out from the strain indicator were merely apparent strains indicated by the strain gages placed in biaxial strain fields which differed from the biaxiality of the strain field in which the gages were calibrated. Although the correction for transverse strain effects should be made to convert these apparent strains into true strains, it was found that the accuracy of the strain-measurements, the cross-sensitivity factor of the gages and the biaxiality of the strain fields did not seem to justify this correction. Consequently, the strain-readings taken from the experiments were directly used for plotting the test curves without being corrected for transverse strain effects. The errors involved were quite small and could be neglected.

Figures 22, 23 and 24 show the results of the strain-measurements made in assembling the ring models. The plotted strain values represent the average tangential strains as measured at four chosen points around the outer circumference of each ring model. These measured strains are compared with the theoretical values, plotted in dash lines, directly computed from Equation (3.27) with $p = 0$.
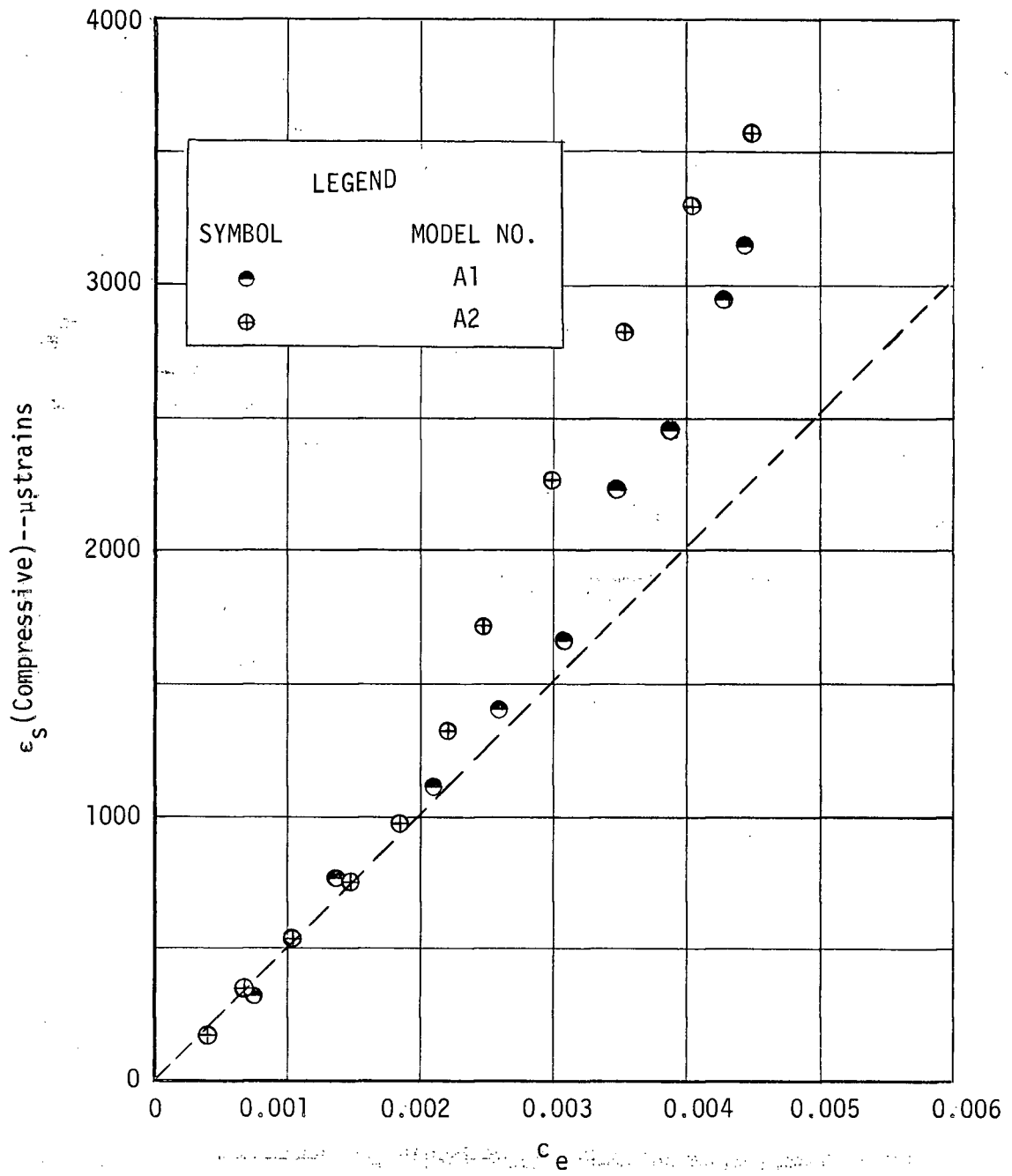
FIGURE 22   Results of Strain-Measurements Made in Assembling
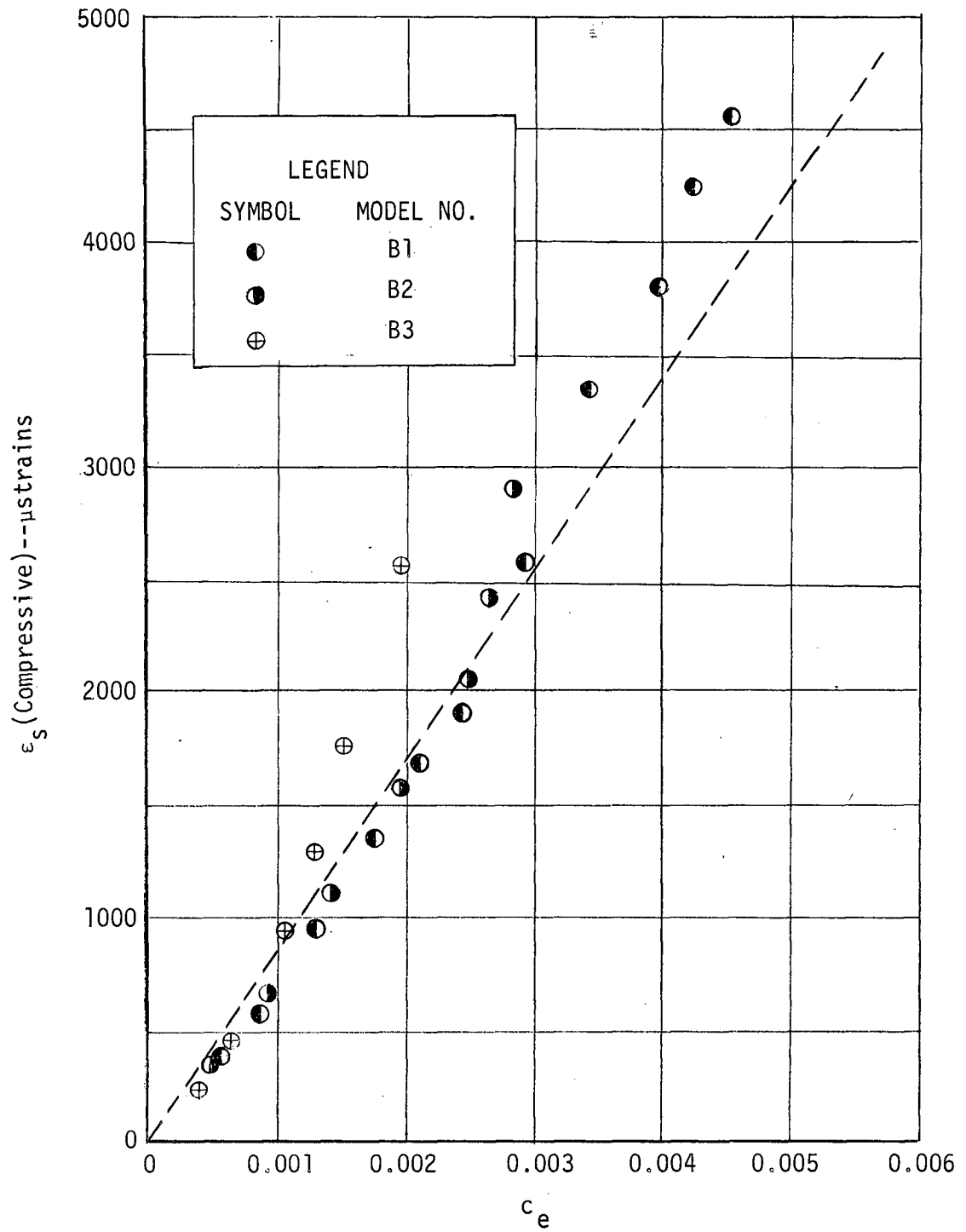Wide-Ring Models

FIGURE 23   Results of Strain-Measurements Made in Assembling
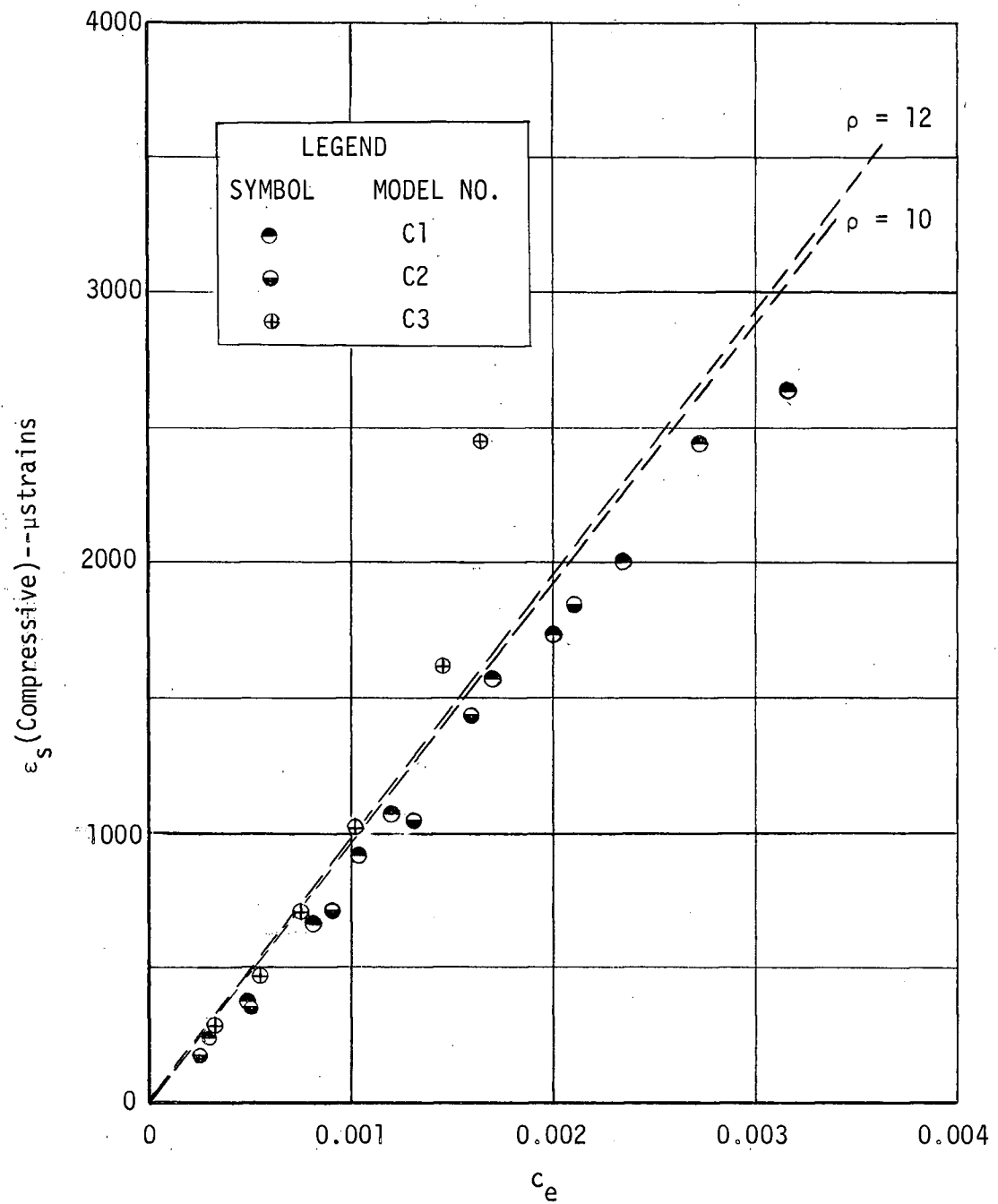Mid-Ring Models

FIGURE 24 Results of Strain-Measurements Made in Assembling
Narrow-Ring Models

In Figures 25, 26 and 27 are pressure-tangential strain curves for various ring models. During pressure tests, strain-measurement was taken at every 1,000 psi. throughout the pressure range up to 10,000 psi. for all ring models except No. A2 and No. C3. The strain gages bonded on these two models failed to perform normally when the hytrostatic pressures applied had intensities over 4,000 psi. and 5,000 psi. respectively. The strain-measuring operations for Model A2 and C3 were thus forced to stop at these pressures. Again, for the purpose of comparison, in addition to the test curves, the computed curves are also shown in dash lines in the figures. It should be noted that the corrections for the flange-movement effects on ring deformations were made to the computed curves rather than to the test curves. In every pressure test, the average stretch of studs at each pressure increment was obtained, through calibration, from the tensile strains which were indicated by the strain gages installed in three of the studs. This stud stretch represented the associated flange movement and was converted into the end displacement of ring by using a geometrical relation similar to that expressed by Equation (4.1). Finally, Equation (3.27) was employed to compute the theoretical strain values.

6.2 Comparisons Between Experimental Data and Theoretical Values

An inspection of the ε_s-readings taken in assembling the ring models showed that up to points where yielding stresses were produced, they were in fair agreement with the calculated values, and the differences were too small to be significant.

On the other hand, from Figures 25, 26 and 27, it was seen that the strain values measured in the pressure tests were appreciably
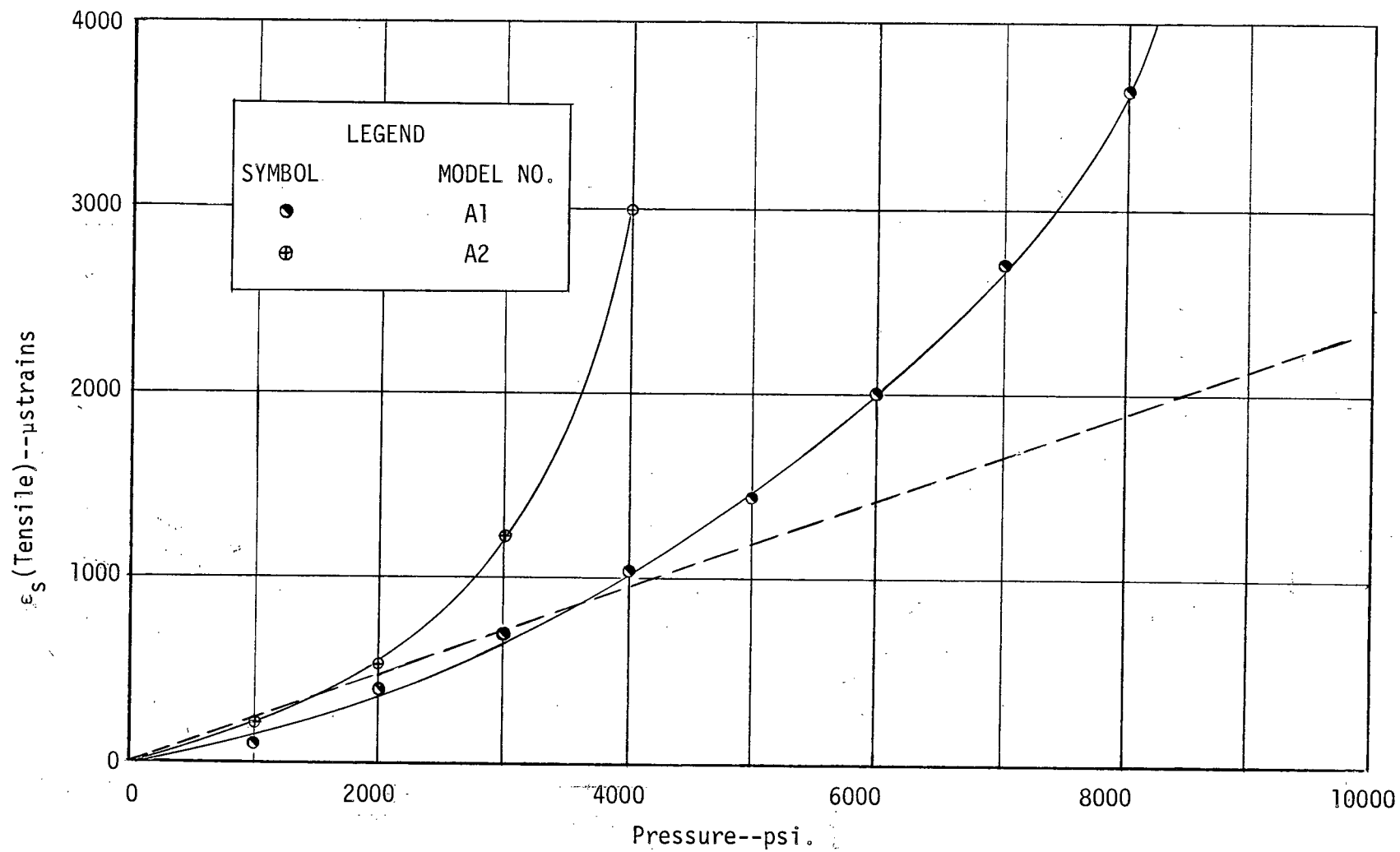
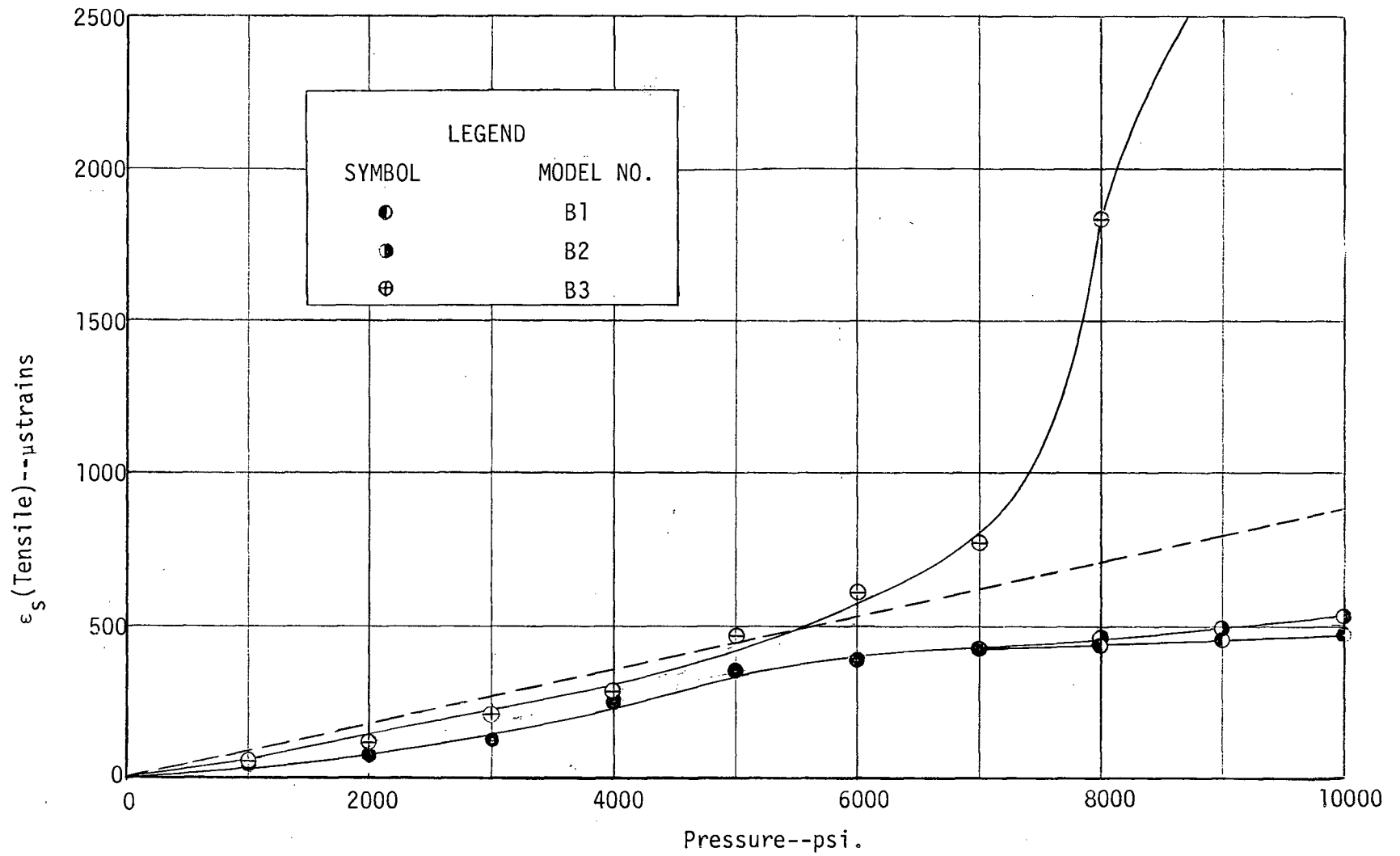FIGURE 25. p-ϵ_s Curves for Wide-Ring Models

FIGURE 26 p-ε_s Curves for Mid-Ring Models

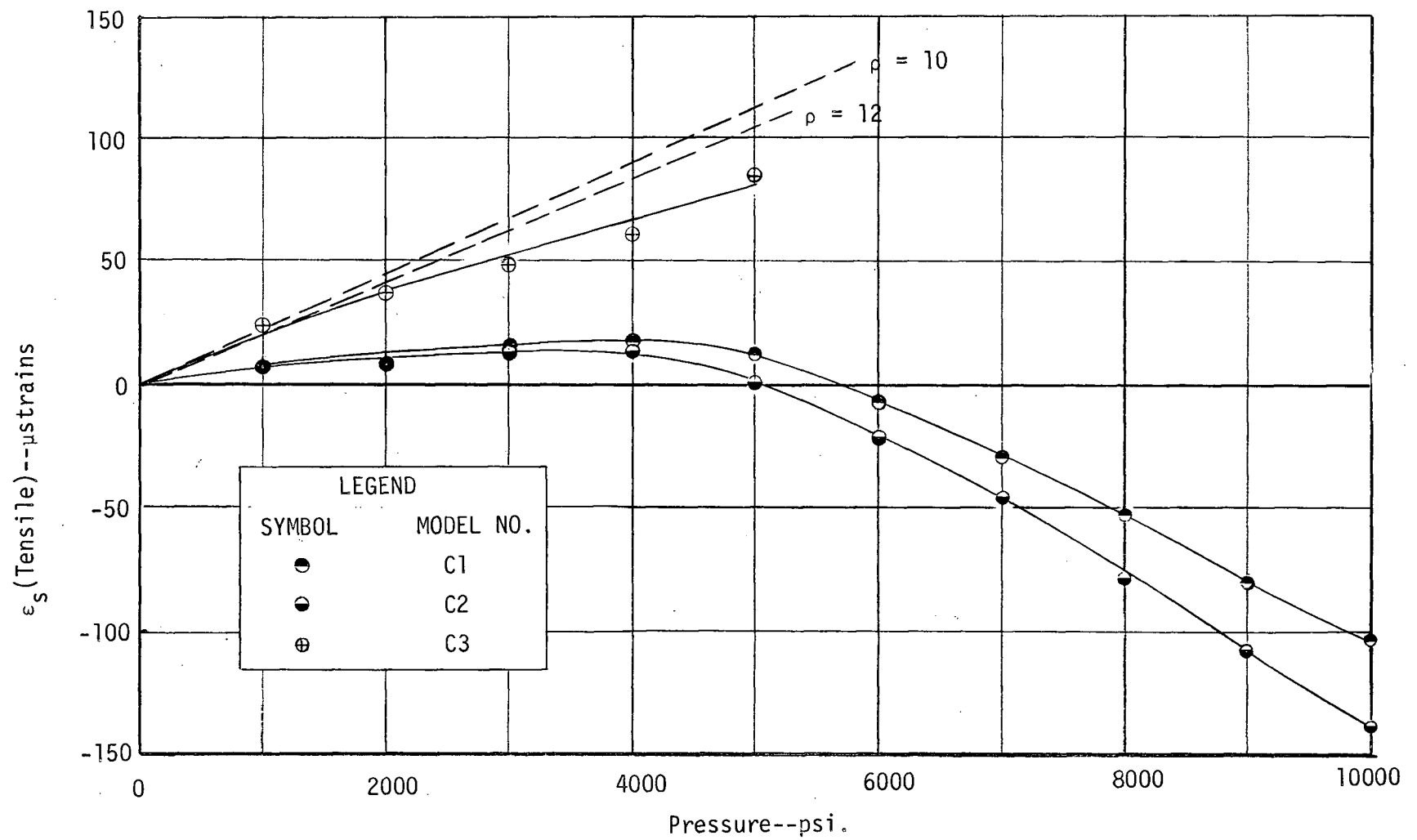FIGURE 27 p-ε_s Curves for Narrow-Ring Models

different from that predicted by the theoretical calculations. Attempts were made to explain the discrepancies, and the following probable reasons are advanced.

The most significant fact in explaining the unsatisfactory experimental results was that at the very beginning of every pressure test, the resultant of the sealing pressure exerted on a ring bevel, N, would act at points along the center circle of the bevel. As the intensity of applied pressure increased during the test, the ring wall was graduately coned by the increasing bending due to pressure, and shifting of the sealing force from the center circle toward the inner edge of the bevel resulted. This violation of the assumed end conditions would have made the measured strain values smaller than that predicted by the analytical solutions, in which the sealing force was assumed to act at the extreme outer edge of the ring bevel. Furthermore, it was certain that the effect of the violation of the assumed end conditions was larger for the narrow- and mid-ring models than for models of the wide-ring series.

Another suspicion was borne out to some extent, by noting that the results of the pressure tests on annealed models approximated to the theoretical values better than that on the cold-drawn models. It was possible that the axial grain-alignment formed in cold extrusion, if not relieved by annealing, would have had certain influence on the behaviours of the ring models made of cold-drawn tubing.

Finally, it was noted that in the assembled-state, all the ring models were being subjected to compressive stresses well beyond the proportional limits of the model materials, and were in the strain-hardening regions [15]. Figure 28 shows the typical stress-strain diagram for mild steel, along with the unloading and reloading lines

originated in the strain-hardening region.

Stress

Strain

Region of
Proportionality

Strain-Hardening Region
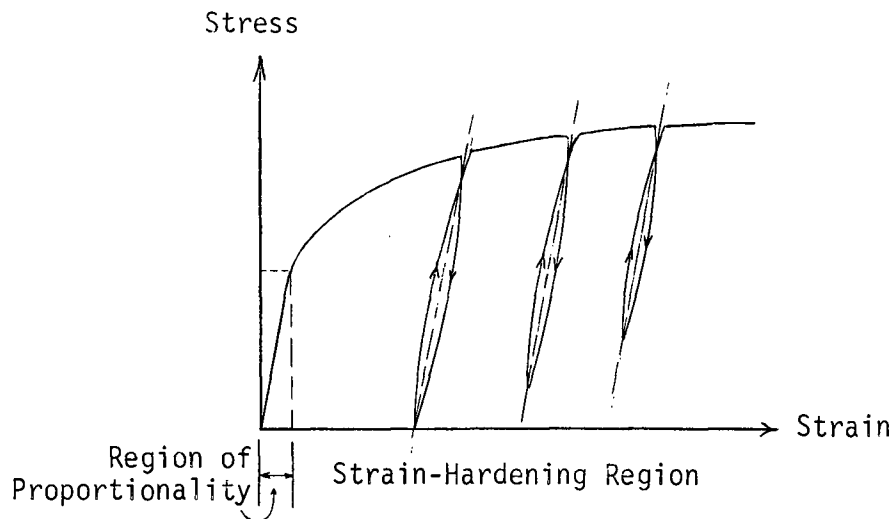
FIGURE 28 Typical Stress-Strain Diagram for Mild Steel

Although these unloading and reloading lines can be approximated by straight lines that are parallel to the straight line in the region of proportionality, they are actually slightly curved lines forming narrow loops. Hence, it seemed to be understandable that the ring models would not have had perfectly elastic distortions during the pressure tests.

In spite of the reasons mentioned above, it was still difficult to understand why in testing the cold-drawn models of the narrow-ring series, when the applied hydrostatic pressures were greater than 5,000 psi., the tangential strains of the ring models decreased as the pressure increased. No explanation had been found for the abnormal behaviour of these two models.

6.3 Observations Made During Tests

A few observations in connection with the performance characteristics of the ring models were made during the tests. These observations are summarized as follows:

Sealing Capacity

When properly assembled, every ring model used in this investigation could create and maintain a perfect pressure-tight seal throughout the pressure range up to 10,000 psi. However, the uniform tightening of studs in assemblies was found to be of utmost importance for the sealing capacities of the ring models. Difficulty in providing efficient initial sealing was encountered in one of the pressure tests when the ring model being tested had been shifted out of place in assembly.

Effect of Cycling Pressure Load

A series of pressure tests were conducted on ring models A1, B1, B2, B3 and C1 to cycle the hydrostatic pressures applied on the assembled ring models from zero to 10,000 psi. This was done for more than twenty times for each of the ring models without leakage. Furthermore, the fact that no re-tightening of studs was ever found necessary during this series of tests gave conclusive evidence that a joint employing the double-cone ring gasket could be subjected to cycling pressure load without periodical field maintenance.

Permanent Deformations After Tests

More or less, every tested ring model was found permanently deformed. The amount of permanent deformation was approximately proportional to the α-value of the ring model. For models of the wide-ring series, the permanent deformations after tests were as large as could be detected by the coned ring walls, as illustrated in Figure 29. On the other hand, for models of the other two series, the permanent deformations were quite small and could not be detected visually.

Re-usability

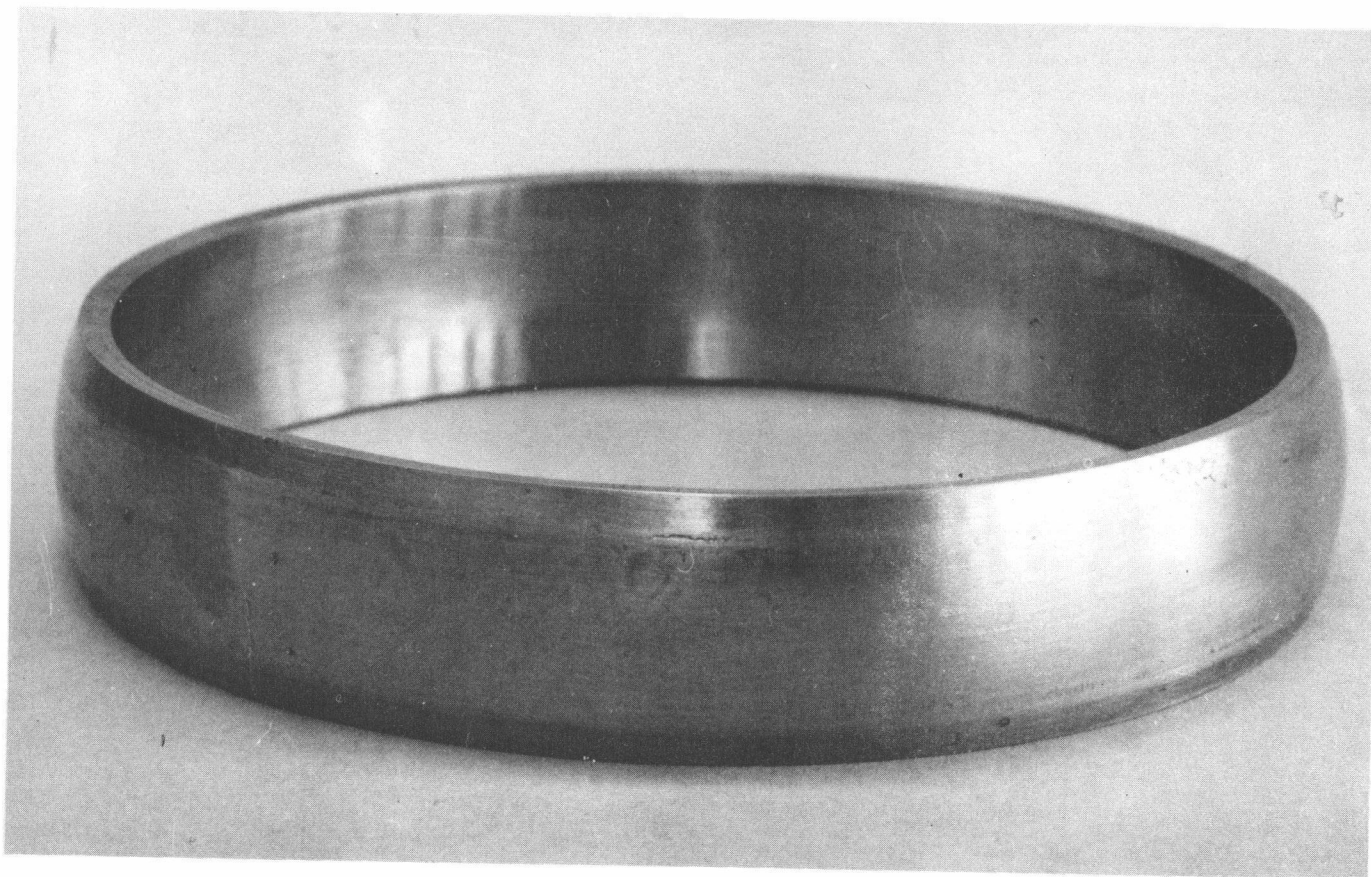Three of the ring models, A1, B1 and B2, had been successively

FIGURE 29   A Wide-Ring Model After Tests

subjected to assembly processes and pressure tests for more than four times, and no leakage was observed. This effectively demonstrated the outstanding re-usability of the double-cone ring gaskets. Additionally, it was noted that the permanent deformations in the ring walls, which resulted from previous tests, had no practical effect on the sealing capacities of the ring models when re-used.

Stud Elongations

The excessive bolt strains often associated with the compression type high-pressure gaskets were not found in this investigation. At 10,000 psi., the total stud elongation averaged only 0.0015 in. It was found that, the stud elongations in pressure tests were directly proportional to the applied hydrostatic loads.

6.4 Design Criteria on Double-Cone Ring Gaskets

Experience with this investigation resulted in a few criteria on the design of the double-cone ring gaskets. These criteria are reported in this section.

The focal point around which the problem of designing a double-cone ring gasket is to provide the initial seal which is imperative to the successful application of the gasket. As the assembly process of the gasket is completed, the intensity of the sealing pressure exerted on the contact surfaces of ring bevels and flanges must be high enough to obtain a perfect metal-to-metal contact; for accomplishing the initial seal provided by the plastic flow of gasket material into the tool marks and imperfections on the flange facing. Theoretical calculations using Equation (3.21) showed that in this investigation, the minimum value of the initial sealing pressures exerted on the assembled ring models was

in the order of 24,000 psi. for Model B1. Hence, it is estimated, on the conservative side, that 25,000 psi might be taken as the required bearing load to ensure an efficient initial seal for the double-cone ring gaskets made of cold-drawn SAE 1020 mild steel. As for the annealed gaskets, the required bearing load could be considerably reduced.

The amount of unsupported-area of a double-cone ring gasket, and hence the inherent ability of the gasket to be pressure-energized in working, is controlled by its pressure-contact ratio, k. Theoretically, assuming no flange-movement occurs and the ring not to yield, a pressure-contact ratio of one seems to be sufficient to ensure a good seal. However, this value is practically too small for two reasons. The first one is that the flange separation cannot be avoided in every high-pressure joint, which tends to relieve the bearing loads on the ring bevels. The second reason is due to the fact that the plastic flow on the ring bevel, which is essential for an efficient seal, has a tendency to re-distribute the high localized sealing pressures to the adjacent parts. Therefore, higher pressure-contact ratios are necessary to be selected in designing the double-cone ring gaskets to compensate these effects. In this investigation, two values of pressure-contact ratio, 3 and 6, were tested, both were found satisfactory.

Of the design parameters of the ring, the ratio of mean radius to thickness, ρ, is the dominant factor in determining the thickness of ring wall (see Equation (4.2)). Since the thickness is affected by two conflicting requirements; the sufficient strength and the ease with which the ring gasket can be pressure-energized; the selection of ρ-values in designing the double-cone ring gaskets becomes a compromise matter. ρ-Values in the range from 10 to 15 were used in this investigation, and

the resultant ring gaskets were found adequate for flanges with 3 in. bore.
It is apparent that the upper limit of ρ-values can be extended when
flanges with larger bore sizes are to be joined. As for the ratio of
half-width to thickness, α, although values ranging from 1 to 3 were
chosen in this investigation and found acceptable, it seems that there
will be no reason to use a α-value higher than 1 as long as good sealing
is the only consideration.

Relatively tolerant in design is the inclination angle of ring
bevel, θ. A literature research [6][7][16][18] showed that angles of 12.5°,
23° and 30° from the vertical have been used in practice for the double-
cone ring gaskets or the similar ones. Although smaller inclination
angles would impose closer manufacturing tolerances, 12.5° was adopted in
this investigation for approximating the cross-sections of the longitudinal
slivers of ring models to the rectangular shape assumed in the theoretical
analysis.

The ring models used in this investigation were machined from
cold-drawn and annealed tubing sections of SAE 1020 steel. The results
of the pressure tests indicated no difference that would warrant any
definite statement regarding the effect of annealing on the pressure-
energizing capacity of the double-cone ring gasket. However, the effect
of annealing did appear in the degree of surface finish of ring bevels
that could be produced by the machining tools, and would make the plastic
flow of gasket material easier to improve the sealing.

Although the design considerations for the flanges joined by
the double-cone ring gaskets is beyond the scope of this investigation.
It is recommended that these flanges should be made of metals harder than
the gasket material for avoiding permanent set on the contact surfaces,

and should butt face-to-face in assembly, as in this investigation, for the reason that the bolt load applied in assembly can be partly carried by the flange faces, and hence, the thickness of the gasket can be considerably reduced from the strength viewpoint.

CHAPTER VII

CONCLUSIONS AND RECOMMENDATIONS

7.1 Summary of Conclusions

Definite conclusions could not be readily drawn from study of a limited scope such as reported in this thesis. The principal value of the present study was in providing a basis for further investigations of the pressure-energized type of ring gaskets. The results of the study did, however, point out some important merits of the double-cone type ring gaskets, and they suggested certain criteria on design.

The following statements briefly summarize the general results of this investigation.

1) The acceptability of the principle of unsupported-area in high-pressure gasket design was confirmed.

2) The advantage of using the double-cone ring gaskets as static seals was justified. Although, in this investigation, hydrostatic pressure up to only 10,000 psi. had been sealed successfully, there was every indication that the double-cone ring gaskets could be employed at still higher pressures.

3) Experiments carried out with various models revealed that the optimum design properties of the double-cone ring gasket were quite tolerant to changes in proportions.

4) The focal point in designing the double-cone ring gasket should be to provide an adequate initial seal, since the sealing capacity of the gasket induced by pressure-energization did increase with the intensity of the contained pressure at an efficient rate.

5) In the course of experimental work, it was noticed that the satisfactory application of a double-cone ring gasket could be secured only when extreme care was used in assembling the gasket into proper position in the pressure enclosure.

6) The inherent sealing capacity and the re-usability of a double-cone ring gasket were not affected by limited plastic deformation in ring walls.

7) A mathematical treatment for the elastic behaviours of the double-cone ring gaskets was examined, and the distortion of the ring gasket under applied loads was formulated.

8) Strains on the outer circumferences of the ring gasket models under working conditions were measured with variable-resistance strain gages. In assembling the ring models, the measured values agreed fairly well with that predicted by theoretical calculations. However, great discrepancies were found between the experimental data taken in pressure tests and the computed values due to plastic effect and violation of the assumed boundary conditions in the tests.

7.2 Recommendations

It might be of value to investigate the elastic behaviour of the double-cone ring gasket by using numerical methods. Since a ring gasket is an axisymmetrical solid generated by the revolution of one of its cross-sections about the axis, as in Figure 30 where cylindrical coordinates r, θ and z are used, and is subjected to a given axisymmetric loading system, the stress components in such a ring gasket are all independent of θ, and can be expressed in terms of two stress functions
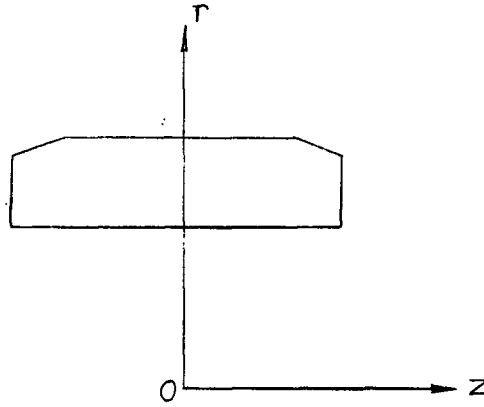
FIGURE 30 A Cross-section of the Double-cone Ring Gasket
with Cylindrical Coordinates $r\theta z$

ψ_1 and ψ_2 in the forms derived by Southwell [19]

$$\sigma_r = \frac{1}{r}\left(\frac{\partial\psi_1}{\partial r} + \frac{\partial\psi_2}{\partial r}\right) - \frac{1}{r^2}\left[\psi_2 + (1-\mu)\psi_1\right]$$

$$\sigma_\theta = \frac{\mu}{r}\frac{\partial\psi_1}{\partial r} + \frac{1}{r^2}\left[\psi_2 + (1-\mu)\psi_1\right]$$

$$\sigma_z = -\frac{1}{r}\frac{\partial\psi_2}{\partial r} \quad \text{and} \quad \tau_{zr} = \frac{1}{r}\frac{\partial\psi_2}{\partial z}$$

where, ψ_1 and ψ_2 are functions of r and z only, and must satisfy the
following simultaneous equations

$$\frac{\partial^2\psi_1}{\partial r^2} - \frac{1}{r}\frac{\partial\psi_1}{\partial r} + \frac{\partial^2\psi_1}{\partial z^2} = 0$$

$$\frac{\partial^2\psi_2}{\partial r^2} - \frac{1}{r}\frac{\partial\psi_2}{\partial r} + \frac{\partial^2\psi_2}{\partial z^2} = \frac{\partial^2\psi_1}{\partial z^2}$$

Then, on a square mesh drawn to cover the gasket cross-section shown in
the figure, these governing equations can be converted into corresponding
finite-difference equations and solved by relaxation process. By
selecting the mesh size to a smallest possible limit and using the
high-order finite-difference approximations [20], solutions with great

accuracy could be expected. However, in performing this numerical analysis, some special points of the relaxation techniques concerned with the satisfaction of the appropriate boundary conditions must be noted [19], and a large amount of labour has to be devoted.

The numerical solutions for three types of thick axisymmetric plate of varying geometry had been obtained by Kenney and Duncan [21], and were compared with the parallel experimental stress analyses using the frozen-stress technique. It might be similarly desirable to carry out a three-dimensional photoelastic study of the stress distribution in the double-cone gasket for comparing with the result obtained by the numerical method described in last paragraph.

REFERENCES

1. Bridgman, P. W., The Physics of High Pressure, G. Bell and Sons, Ltd., London, 1931, p. 30-35 and p. 78-97.

2. Bridgman, P. W., "The Technique of High Pressure Experimenting", American Academy Arts and Sciences Proceedings, Vol. 49, 1913, p. 628.

3. Bridgman, P. W., "High Pressures and Five Kinds of Ice", Journal of the Franklin Institute, Vol. 177, 1914, p. 315.

4. Bridgman, P. W., "Breaking Tests Under Hydrostatic Pressure and Conditions of Rupture", Philosophical Magazine, Series 6, Vol. 24, 1912, p. 63.

5. Bridgman, P. W., "General Survey of the Effects of Pressure on the Properties of Matter", Proceedings of the Physical Society, Vol. 41, 1929, p. 341.

6. Freese, C. E., "Mechanical Design Problems Connected with Ammonia Synthesis", a paper presented at the ASME Petroleum Mechanical Engineering Conference, September, 1956, ASME Paper No. 56-PET-1.

7. Freese, C. E., "Here are Ammonia Plant Design Tips", Petroleum Refiner, January, 1957, p. 193.

8. Everett, M. H. and Gillette, H. G., "Static O-Ring Seals", Seals Book, a penton publication of the Machine Design, 1961, p. 100.

9. Dunkle, H. H. and Gastineau, R. L., "Metallic Gaskets", Seals Book, a penton publication of the Machine Design, 1961, p. 103.

10. Den Hartog, J. P., Advanced Strength of Materials, McGraw-Hill Book Company, Inc., New York, p. 164-165.

11. Timoshenko, S., "Strength of Materials, Part I", Third Edition, D. Van Nostrand Company, Inc., Toronto, 1955, p. 113-118 and p. 170-171.

12. Levy, S., "Shear and Bending of the Walls of Short Cylindrical Shells", a paper presented at the Winter Annual Meeting of the ASME, November-December, 1964, New York, ASME Paper No. 64-WA/MD-9.

13. Dally, J. W. and Rilley, W. F., Experimental Stress Analysis, McGraw-Hill Book Company, New York, 1965, p. 366-476.

14. Dove, R. C. and Adam, P. H., Experimental Stress Analysis and Motion Measurement, Charles E. Merrill Books, Inc., Ohio, 1964, p. 50-281.

15. Phillips, A., <u>Introduction to Plasticity</u>, the Ronald Press Company, New York, 1956, p. 3-4.

16. Eichenberg, R., "Design of High-Pressure Integral and Welding Neck Flanges with Pressure Energized Ring Joint Gaskets", Journal of Engineering for Industry, May, 1964, p. 199.

17. Eichenberg, R., "High-Pressure Wellhead Equipment -- Design Considerations for AWHEM 15,000-psi. Flanges", Mechanical Engineering, Vol. 80, No. 3, p. 66.

18. Brooks, R. C., "High-Pressure Wellhead Equipment -- Wellhead Connections", Mechanical Engineering, Vol. 80, No. 3, p. 63.

19. Allen, D. N. de G., <u>Relaxation Methods</u>, McGraw-Hill Book Company, Inc., New York, 1954, p. 134-144.

20. Wang, Chi-Teh, <u>Applied Elasticity</u>, McGraw-Hill Book Company, Inc., New York, 1953, p. 122.

21. Kenny, B. and Duncan, J. P., "An Assessment of Methods of Three Dimensional and Experimental Stress Analysis", departmental paper of the Department of Mechanical Engineering, University of British Columbia, December, 1966.